

Politecnico di Torino

In collaboration with: Universidad de Huelva, Escuela Técnica Superior de Ingeniería, ETSI

Master's Degree in Environmental and Land Engineering Climate Change 2024/2025

Graduation session: November 2025

Spatial modelling of solar irradiation and evapotranspiration for the improvement of the cultivation of *Artemisia umbelliformis* in Aosta Valley

Supervisors:

Candidate:

Prof. Marta Tuninetti

Sara Bongiovanni

Prof. Igor Rapp Arraras

Prof. Paolo Dabove

Dr. Elena De Petrillo

Abstract

The *Artemisia umbelliformis*, traditionally used to produce the genepì liqueur, represents one of the most valuable non-timber alpine resources in the Western Alps. This study presents an innovative methodology of modelling solar irradiation and evapotranspiration, considering the complex topography of the Aosta Valley (Italy) in as much detail as possible to improve the use and cultivation of the herbaceous plant.

Starting from high-resolution digital elevation models (2 m x 2 m) and using ArcGIS "Raster/Area Solar Radiation", the spatial and temporal modelling of solar irradiation in the area of agricultural interest was performed, incorporating aspect, slope and topography shading, thanks to the calibration of atmospheric transmissivity and diffusivity coefficients against PVGIS data. The resulting layers were coupled with FAO-56 Penman–Monteith methods for the calculation of terrain-aware reference evapotranspiration (ET_o).

By approximating the correct crop coefficient and thus obtaining the potential evapotranspiration, the study estimated the water demand of each cultivated field and consequently the irrigation requirements for the month under consideration.

Results show that the already existing *Artemisia umbelliformis* fields correspond to micro-areas characterized by higher solar exposure and evapotranspiration compared to the average in the study area, which indicates favourable exposure and microclimatic conditions.

This methodology represents a replicable approach for assessing water balance and cultivation suitability in alpine environments, evaluating both the already existing fields of the cultivation of interest as well as suitable future cultivation areas.

Keywords

Reference evapotranspiration (ET_o); *Artemisia umbelliformis* (A.U.); Geographic information system (GIS); Solar radiation; Irradiation; Temperature; Direct radiation; Diffuse radiation; Cultivation fields; Digital Terrain Model (DTM); FAO; Penman-Monteith; Interpolation; Topography; Crop coefficient; Potential evapotranspiration; Water deficit.

Summary

	1.1. Context	5
	1.1.1. Cultivation requirements	5
	1.1.2. Study area	6
	1.2.2. FAO-56 Penman-Monteith ET₀ equation	9
	1.2.3. Sensitivity of ET to solar radiation	.12
	1.3. Topographic effects on solar radiation distribution	.13
	1.3.1. GIS solar tools	.14
	1.3.2. Tool Calibration	.15
	1.3.3. New developments in the calibration method	.16
	1.4. Goals and attended results	.17
2.	Material	.18
3.	Methodology	.19
	3.1. Calibration and estimation of transmissivity and diffusivity coefficients	.19
	3.2. Spatial analysis and radiation modelling over agricultural area.	.21
	3.2.1. Delimitation of the potential agricultural area	.21
	3.2.2. Spatial interpolation of coefficients	.22
	3.2.3. Real radiation maps over agricultural area	.26
	3.3. Calculation of potential evapotranspiration (ET _o)	.30
	3.3.1. Calculation of all the parameters needed in the final formula	.30
4.	Results	.37
	4.1. July's results	.39
5.	K _c calculation	.42
6.	Precipitation Data Processing and Water Balance Assessment	.44
	6.1. Water Deficit Calculation	.45
6.	Conclusion	.49
Di	bliography	5 1

Index of figures

Figure 1. Artemisia umbelliformis, https://zermattflora.net/content/artemisia-umbe	lliformis-
yellow-genipi/	_
Figure 2. Geographic location of the Aosta Valley in northwestern Italy. The map sh	
position of the study area within the regional and national context	
Figure 3. Alpine morphology and the main longitudinal valley of the Dora Baltea riv	
Aosta Valley https://www.alamy.it/fotos-immagini/mappa-de	
d%E2%80%99aosta.html?sortBy=relevant	6
Figure 4. Diagram of evapotranspiration components and controlling factors. FAO-56	(Allen et
al., 1998)	7
Figure 5. Flowchart of ET _o calculation process	
Figure 6. Area of agricultural interest (green), Artemisia umbelliformis fields (red)	
Figure 7. Training points (light blue), Validating points (purple)	
Figure 8. Visual representation of ti interpolation in the agricultural area	25
Figure 9. Visual example of January diffuse radiation with transmissivity coefficient	
diffusivity coefficient 0.5 [kWh/m²]	
Figure 10. Direct irradiation [kWh/m²]	
Figure 11. Diffuse irradiation [kWh/m²]	
Figure 12. Global irradiation [kWh/m²]	
Figure 13. Visual representation of the minimum temperature of January [°C]	
Figure 14. Visual representation of the maximum temperature of January [°C]	
Figure 15. Visual representation of the mean temperature of January [°C]	
Figure 16. R _s representation [MJ/m²day]	32
Figure 17.R _{ns} representation [MJ/m²day]	32
Figure 18. Visual representation of e _s [kPa]	34
Figure 19. Visual representation of ea [kPA]	34
Figure 20. Visual representation of Pressure P [kPa]	36
Figure 21. Histogram of the irradiation of the study area during January	37
Figure 22. January's reference evapotranspiration [mm/day]	
Figure 23. Histogram of January's Reference Evapotranspiration.	38
Figure 24. Irradiation of July [MJ/(m²day)]	
Figure 25. Histogram of the irradiation of the study area during July	39
Figure 26. July's Reference Evapotranspiration [mm/day]	40
Figure 27. Histogram of July's Reference Evapotranspiration	
Figure 28. Visual representation of the water deficit in the study area [mm/day]	45
Figure 29. Visual representation of positive, negative and null D values in the	area of
agricultural interest	
Figure 30. Visual representation of water deficit in the study area [mm/day]	47
Figure 31. Visual representation of positive, negative and null D values in the	area of
agricultural interest	48

Index of tables

Table 1. Different spline parameters	23
Table 2. Different Kriging parameters	24
Table 3. Comparison of the different methods	24
Table 4. Comparison between perennial aromatic herbs	42
Table 5. Crop coefficients	42
Table 6. Correction of Kc _{mid}	43
Table 7. Correction of Kc _{mid} with standard wind velocity	43
Table 8. Water deficit conditions of all the existing fields using a Kc _{mid} of 1	45
Table 9. Water deficit conditions of all the existing fields using a Kc _{mid} of 0.8	47

1. Introduction

1.1. Context

The Artemisia umbelliformis (A.U.) (Figure 1) is an herbaceous alpine plant belonging to the Asteraceae family, and its flowers are used to produce an alcohol-based infusion called genepi in Italian (Comino et al., 2014). Some regions, such as Savoie and the Aosta Valley, use several hundred kilograms of dried plants annually. This strong demand of the herbaceous plant represents a real opportunity for the development of mountain crops, which also helps to prevent the genetic impoverishment of this plant in the wild (Rey et al., 2002).



Figure 1. Artemisia umbelliformis, https://zermattflora.net/content/artemisia-umbelliformis-yellow-genipi/

1.1.1. Cultivation requirements

In nature this plant grows at high altitudes between 1200 and 3100 m a.s.l. where the environment is characterized by low temperatures, heavy precipitation and long winters. Some topographic and climatic variables determine its spatial distribution which are temperature annual range, topographic position index, temperature seasonality and altitude. The importance of temperature variables (diurnal and annual range, seasonality) for the model of A.U. presence is consistent with the fact that temperature is a major constraint on plant species in mountain environments with an extended period of freezing risk and a short growing season (Korner, 2003) (Fontain et al., 2024). The aspect plays a crucial role in the distribution and growth of this specie:

- South-facing slopes tend to favour biomass accumulation.
- Noth-facing slopes tend to delay phenomenological development due to the longer snow cover (Korner, 2003).

For a successful cultivation instead, specific conditions are required: the plant grows better at elevations above 1600 m and requires drained soils and south facing exposition. (Binet et al., 2011). White genepi` also needs a mountain climate to reach its optimal growth in cultivation. (Rev et al., 2002). It presents a decrease in mortality rate with altitude.

Neutral or calcareous, light, well-drained soils, as well as grassland stubble, are the best options. Drainage can reduce the plant mortality by preventing the development of fungal diseases, while heavy soils present a higher risk of water stagnation that can cause the appearance of devastating fungi that can destroy the crop. Soils that are too rich are not recommended.

This herb is usually planted in early June and harvested the second year. During the month of July, the plant is in full bloom, i.e. at the time of maximum vegetative and transpiration activity. To end the cultivation a final harvest is done in early summer of the third year, or, in exceptional cases, the crop could remain for a fourth year. (Bondaz et al., 2021)

1.1.2. Study area

High mountain areas are particularly interesting for the study through a spatial, interdisciplinary approach. In these areas, crests and summits are particularly harsh environments and ecological conditions may change on small spatial scales in relation to micro-topography and sharp gradients in abiotic variables such as substrate granulometry (rocks, stones, bare soil) or microclimatic conditions (Fontain et al., 2024).

The Aosta valley is characterized by a mountainous morphology. Its landscape is dominated by some of the highest peaks in Europe such as Monte Rosa (4634 m), Grand Paradiso (4061 m) and Mont Blanc (4810 m). It is also the only Italian region to be completely located in the Alpine arc. (Figure 2)

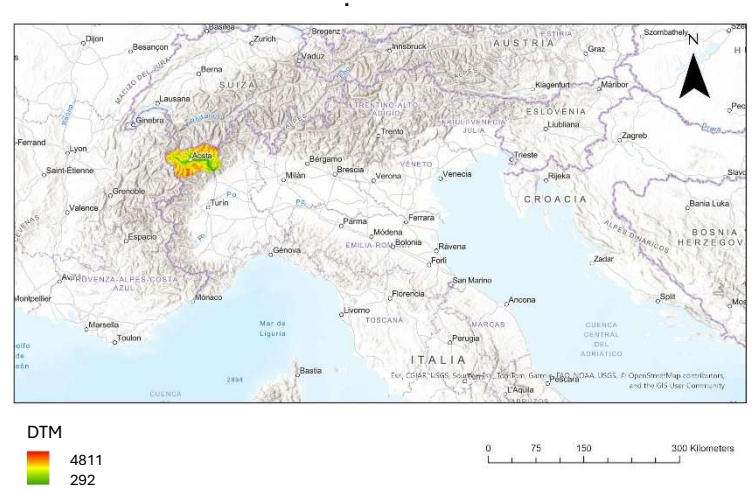


Figure 2. Geographic location of the Aosta Valley in northwestern Italy. The map shows the position of the study area within the regional and national context.

The territory is developed in a longitudinal way following the Dora Baltea River which creates the main valley. Connected to this, many other tributaries form additional, smaller valleys (Figure 3).



Figure 3. Alpine morphology and the main longitudinal valley of the Dora Baltea river in the Aosta Valley https://www.alamy.it/fotos-immagini/mappa-della-valle-d%E2%80%99aosta.html?sortBy=relevant.

This morphology produces a variety of slopes, landform orientations, and elevation, which evokes sharp gradients in solar radiation, snow retention, and soil and climate characteristics. The valley floor hovers around 500–600 m a.s.l. and the orientation is systematically varied. The combination of altitude, slope gradient and aspect thus make the entire radius of the Aosta valley in a particular suitable area for the study of how topography can influence solar radiation, and, consequently, the evapotranspiration, which plays a key role in the crop growth.

1.2. Evapotranspiration concepts and its role in crop water balance

Knowing the variation of the water consumption of a crop or vegetation can help to avoid damages caused by the lack of water. The water requirements of crops are measured using the following Formula (1):

$$\Delta S = Peff + I + Cr - (ETc + D + R) \tag{1}$$

Where ΔS is the water variation of the soil, Peff is the effective precipitation, I stands for irrigation, Cr is the capillary rise, D is the deep percolation, R is the runoff and Et_c is the crop evapotranspiration.

Evapotranspiration is a physical process that strongly characterizes the hydrological cycle (Bosquilia et al., 2019) and is fundamental for the determination of the use of water resources by crops depending on local conditions.

A commonly used approach for estimating the consumptive use of water by irrigated crops is the crop coefficient—reference evapotranspiration (K_c -ET_o) procedure (Allen et al., 1998, 2006).

The term evapotranspiration (ET) is used to describe the combination of two different simultaneous processes of water transport from land surface to atmosphere, evaporation and transpiration, and it is a fundamental component of water balance. It is also strictly linked to ecosystem productivity and sustainability.

Evaporation is a physical process in which a liquid, under certain conditions of temperature and atmospheric pressure, turns into a gas without reaching boiling point. This occurs when molecules at the surface of the liquid, by absorbing thermal energy, obtain sufficient kinetic energy to overcome the intermolecular cohesion forces that hold them together. As a result, these molecules break away from the surface of the liquid and become vapour, ending the endothermic process.

Transpiration is an essential physiological process for plants, during which they release water vapour into the atmosphere, mainly through the stomata, which are small openings on the surface of the leaves, in order to regulate the internal temperature of the plant and transport nutrients. Transpiration rate is influenced by crop characteristics (other than environmental aspects and cultivation practices): different kind of plant can present different transpiration rates.

According to the FAO definition, reference evapotranspiration (ET $_{\rm o}$) is defined as the ET rate from a uniform surface of dense, actively growing vegetation, having specified height and surface resistance, not short of soil water, and representing an expanse of at least 100 m of the same or similar vegetations (Allen et al., 1998, 2006). The concept of the ET $_{\rm o}$ was introduced to study the evaporative demand of the atmosphere independent of crop type, crop development and management practices. If water is abundantly available at the reference surface, soil factors do not affect. The only factors affecting ET $_{\rm o}$ are climatic parameters. From ET $_{\rm o}$ is possible to determinate the crop evapotranspiration ET $_{\rm c}$ using a crop specific coefficient (K $_{\rm c}$) (Zotarelli et al.,2010) (Figure 4).

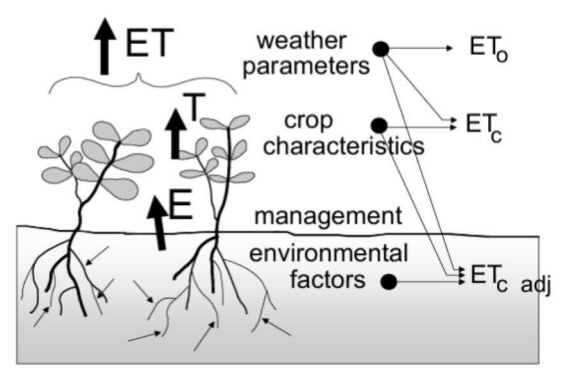


Figure 4. Diagram of evapotranspiration components and controlling factors. FAO-56 (Allen et al., 1998).

1.2.1. Evidence Gap

There is no sign of any publication that attempts to investigate the correlation between reference evapotranspiration and the distribution of *Artemisia umbelliformis* cultivation. Most of the available literature on A.U. deals with ecology, conservation and propagation, with isolated attempts at agronomy, but does not contain a geographically referenced assessment of the relationship between atmospheric water demand and the location of the established fields.

This thesis addresses that gap by producing high-resolution ET_o maps and connecting them with *Artemisia umbelliformis already existing* parcels to provide new information about the plant's needs and to produce the first quantitative base to evaluate how climatic demand interface the cultivation suitability.

1.2.2. FAO-56 Penman-Monteith ETo equation

Despite the many empirical methods that have been developed over the last 50 years for the estimation of the evapotranspiration, starting from different climatic variables, the FAO Penman-Monteith method is the one used in this project. The method has been selected because it closely approximates ET_{o} at the location evaluated, is physically based, and explicitly incorporates both physiological and aerodynamic parameters. Moreover, procedures have been developed for estimating missing climatic parameters. In fact, a disadvantage of the equation is that it requires detailed information that are very difficult to obtain in many cases.

The update equation recommended by FAO uses some assumed constant parameters: the reference surface in this method is a hypothetical grass reference crop with an assumed crop height of 0.12 m, a fixed surface resistance of 70 s m-1 and an albedo of 0.23. (Allen et al., 2006).

In the manual there are different formulas adapted to the available data. In this project the example n.20 of the Spanish version of the manual of 2006 was followed, which include the following Formula (2):

$$ET_o = \frac{0.408 * \Delta * (Rn - G) + \gamma * \frac{900}{(T_{mean} + 273)} * u_2 * (e_s - e_a)}{\Delta + \gamma * (1 + 0.34 * u_2)}$$
(2)

Where:

 ET_o = reference evapotranspiration rate (mm d⁻¹).

 T_{mean} = mean air temperature (°C).

 u_2 = wind speed (m s⁻¹) at 2 m above the ground.

 R_n = net radiation flux (MJ m⁻² d⁻¹).

G = sensible heat flux into the soil (MJ m^{-2} d^{-1}).

 $y = psychrometric constant (kPa °C^{-1}).$

e_a = mean daily ambient vapor pressure (kPa).

e_s = mean saturated vapor pressure (kPa).

 Δ =slope of the saturated vapor pressure curve.

To better understand the main factors of the equation and their derivation, the following flowchart (Figure 5) has been created:

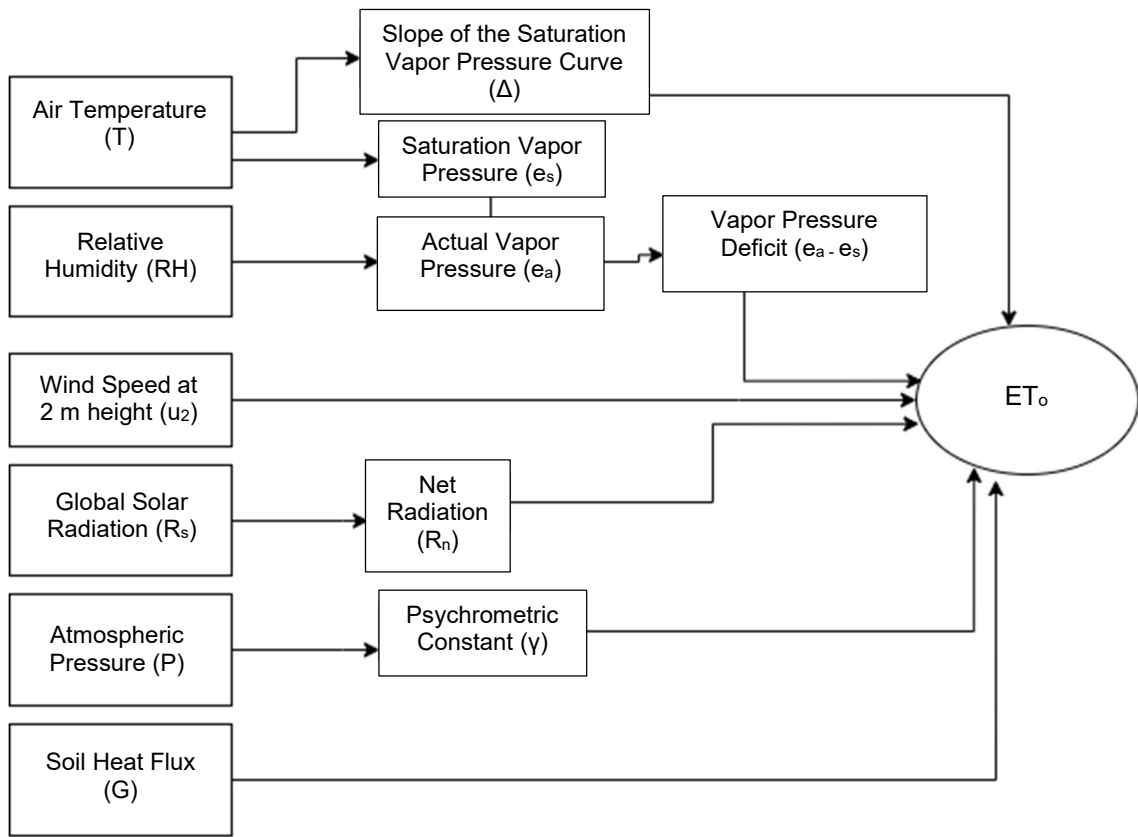


Figure 5. Flowchart of ETo calculation process.

Air Temperature (T): necessary for computing saturation vapor pressure, it is essential in the energy balance. The mean air temperature (°C), calculated doing the average between the daily maximum and minimum temperatures, is a key variable for estimating reference evapotranspiration. When only the mean temperature is available, ET_o could be underestimated because the relationship between temperature and saturation vapour pressure is non-linear.

Air temperature effects the amount of sensible heat of the surrounding air, which transfers energy to the crop and modulates the evapotranspiration process. Therefore, when the weather is warm and clear, the higher thermal energy leads to a major water loss from the soil and plant systems through evapotranspiration.

Relative Humidity (RH): required to estimate the actual vapor pressure ea.

Wind Speed at 2 m Height (u_2) : average wind speed (ms^{-1}) measured at 2 m above the ground level. This influences the turbulent transport of heat and vapor, determining the intensity of the aerodynamic component of ET_o .

When water evaporates, the air layer immediately above the evaporating surface becomes gradually saturated with water vapour. If this saturated air is not replaced continuously with drier air masses, the vapour pressure gradient between the surface and the atmosphere diminishes with a reduction of the evapotranspiration rate. In hot and dry days, the evapotranspiration demand is high due to the amount of available energy under the form of direct solar radiation as well as latent heat and because the dryness of the air. Under those conditions, the atmosphere can retain a considerable amount of water vapour, that is also

removed by wind movements. A high evapotranspiration rates is present. Under humid weather conditions instead, characterized by high humidity of the air and clouds cause the evapotranspiration rate tends to be lower and the wind speed exerts only a minor influence compared with arid conditions where small variations in wind speed may result in larger variations in the evapotranspiration rate.

Global Solar Radiation (R_s): primary source of energy driving evapotranspiration. The potential amount of radiation depends on time of the year and geographic location, varying in latitudes and in different seasons. The actual solar radiation able to reach the evaporating surface is strongly influenced by atmospheric transparency and cloud cover that can absorb major parts of the radiation.

Atmospheric Pressure (P): necessary for determining the psychrometric constant, which affects the energy transfer components in the Penman-Monteith equation. It represents the pressure exerted by the weight of the earth's atmosphere. Evaporation at high altitudes is greater because the low atmospheric pressure. This parameter has a low weight on the formula so an average value for the whole study location is enough.

Soil Heat Flux (G): generally negligible in daily analyses but significant in hourly calculations and under conditions of strong thermal gradients.

Intermediate Variables

Saturation Vapor Pressure (e_s): is calculated as the mean between the saturation vapor pressure at both the daily maximum and minimum air temperatures.

Actual Vapor Pressure (e_a): derived from relative humidity and saturation vapor pressure to estimate the atmospheric moisture content.

Vapor Pressure Deficit (e_s - e_a): a key parameter for quantifying the atmospheric evaporative demand.

Psychrometric Constant (γ): represent the relationship between the partial pressure of water in air and the air temperature allowing the estimation of water pressure using paired dry and wet thermometer bulb temperature readings.

Because atmospheric pressure varies primarily with altitude, representative mean value of pressure is generally assumed for each study area, keeping the same psychrometric constant in each location depending of the altitude.

Slope of the Saturation Vapor Pressure Curve (Δ): determined from the derivative of saturation vapor pressure with respect to temperature; it directly influences the radiative term in the Penman-Monteith equation.

Net Radiation (R_n): These data are not commonly available but can be derived from the difference between the incoming net shortwave radiation (R_{ns}) and the outgoing net longwave radiation (R_{nl}), subtracting them.

In the absence of data, the FAO manual proposes various solutions and formulas to obtain ET_o in an alternative manner, approximating some of them. In this project, as can be seen in chapter 3 focused on the calculation of raster maps of reference evapotranspiration, example 20 of the FAO's manual was followed.

1.2.3. Sensitivity of ET to solar radiation

An operational limitation of the Penman-Monteith method lies in the need to have reliable estimates of the global solar radiation reaching the surface, which plays a fundamental role in the evapotranspiration process.

The solar radiation is a major forcing function of physical and biologic processes on our planet (Dubayah and Rich, 1995). The heterogeneity of incoming solar radiation determines the dynamic of the ecologic, agricultural, and hydrologic processes and therefore the knowledge of the spatial variability of radiation components is very important. (Ruiz-Arias et al., 2009) In the FAO-56 Penman–Monteith formulation the reference evapotranspiration is obtained by combining an energy term to an aerodynamic term, with standardized surface properties. The first term is dominated by the net solar radiation (R_n), which is given by the subtraction of the longwave solar radiation to the shortwave solar radiation. This makes the short-wave input a first-order control on ET_0 . (Allen et al., 2006).

In mountainous terrain, where the topography highly alters solar radiation (slope, aspect, and horizon shading), using point data or spatial interpolation would not be enough to represent correctly the energy term. This was studied by Aguilar et al. (2010), who implemented a topographic solar-radiation algorithm to show how the daily global radiation was different, if obtained through a IDW-interpolation or with a topographic field, studying a large mountain basin in Sierra Nevada.

In the comparison, it turned out that neglecting the relief produces very large errors: on exposed slopes appeared a +42% of radiation than with IDW; in "shadow cells" IDW overestimates the shadow, leading to -1800% as if the IDW model was not able to see the shadow, while the topographic model gives much lower values due to the fact that direct radiation does not reach those cells. Propagating these two versions in the estimation of ET_o , leaded them to obtain a significant result: at the basin scale, neglecting the topographically fields leaded to an average excess of around 61 mm/year of ET_o . The greatest differences were present in summer when radiation has a heavier weight in the energy balance.

These results highlight that corrected radiation inputs are essential for reliable ET_o mapping and water balance assessments in complex terrain. (Aguilar et al. 2010)

1.3. Topographic effects on solar radiation distribution

As explained in the previous paragraph, solar radiation data, although recorded by some weather stations, are not available throughout the territory. Moreover, even when this data are available, they are punctual measurement data and cannot be spatialized with traditional interpolation techniques, as these techniques would neglect determining factors for the estimation of the two quantities under consideration (Dubayah and Rich, 1995).

Solar radiation, in fact, depends on morphological factors such as slope and slope exposure. For this reason, research has tested new computational models and measurement methods based on digital terrain models (DTMs) for the estimation of global solar radiation (Hofierka and Suri, 2002). It should be noted that the same DTM with different resolutions will usually produce different estimations of elevation, slope, aspect and shadowing, especially in complex topographies (Raaflaub and Collins, 2006).

The analysis of DEM-based models changes the proportion of direct and diffuse radiation in the solar global radiation through the shadow-casting effect, for example. (Ruiz-Arias et al., 2009). In other words, the importance of diffuse and reflected components of the radiation grows when the topography increases its complexity (Kondratyev, 1965). In fact, big variability in elevation, slope and aspect create strong local gradients of insolation.

Considering the above, it is essential the use of specific tools that are integrated into Geographic Information Systems, due to their capability of evaluating the effects of morphology on radiation, as well as the possibility to calculate all the components that create the solar flux that hits the Earth's surface.

1.3.1. GIS solar tools

Out of the few existing raster-based models such as GRASS GIS of r.sun or SAGA's potential incoming solar radiation, ESRI's Solar Radiation used in ArcGIS Pro developed by Fu and Rich was selected. It allows, in the command "Raster/Area/point solar radiation", to work with a clear sky model based on a DTM and integrates slope, aspect, and sky discretisation. It also allows the automation of hourly/daily runs via scripts and produces raster outputs ready for map algebra. (León-Sánchez et al., 2025).

GRASS can compute beam, diffuse and reflected radiation components under clear-sky conditions, while simulates overcast conditions using a Linke turbidity factor together with empirical beam and diffuse radiation coefficients, which are obtained from a data bank and calculated from decomposing global radiation measurements from a nearby weather station (Bala et al., 2021). ArcGIS's Solar Radiation uses simplified models, in addition to an easily operable interface with high resolution geospatial graphics. The ArcGIS Pro's Raster Solar Radiation was chosen for its balance of ease of preparation, the possibility of automation, and the compatibility with the subsequent steps.

The most relevant inputs of this tool are orientation, elevation, slope, and atmospheric transmission. The output is global radiation in the energy units of Wh/m² but is also possible to obtain diffuse and direct radiation for the same setting of parameters. The modelling tool is computationally intensive, this means that the process time can run from minutes up to multiple days, depending on the sky size and the raster input.

1.3.2. Tool Calibration

ArcGIS Pro's 'Raster/Area Solar Radiation' tool is a clear-sky, hemispherical viewshed model that reveals atmospheric factors, particularly transmissivity and the diffuse fraction. The accuracy of simulations relies heavily on these values, as well as on slope, aspect, and horizons. Therefore, it is wise to calibrate these factors for local atmospheric conditions. A recent review found that using ArcGIS with default settings can lead to significant differences compared to ground measurements. As a result, the authors suggest calibrating at suitable time scales.

In these tools, is possible to change sky transmissivity and diffusivity parameters, needed for calculating the direct and diffuse insolation as well as select a time series: a year, several months, or days. The diffuse proportion usually ranges from zero to one, with low values of 0.2–0.3 for clear sky conditions. The same happens for transmissivity, but the clear skies values are up to with 0.5–0.7. These two parameters are inversely related.

In this paper different sets of transmissivity (ti) and diffusivity (di) coefficients have been tested in order to obtain direct and diffuse radiation as is explained in the next chapter.

For what concern the other parameters, the time series was calibrated to one month at a time, with a day interval of 7 and an hour interval of 0.25. The Zenith division and Azimuth division have been fixed on 32 and the Standard overcast Sky option was selected.

1.3.3. New developments in the calibration method

Unlike previous methods that consider *ti* and *di* as constant values across all the studied area, such as the ones of Šúri & Hofierka (2004), in this project a monthly calibration of the Raster Solar Radiation atmospheric parameters is carried out, for the entire mountain region of Aosta valley. Earlier strategies like the one used by Kausika et al. (2021), have adjusted these parameters based on meteorological station records.

Here, an average year of direct and diffuse horizontal irradiation from PVGIS following a 2-km grid was calculated, in all the area of the region. At these grid points, Area Solar Radiation in ArcGIS was run using different sets of transmissivity (ti) (0.20, 0.40, 0.60, 0.80) and diffusivity (di) (0.5).

Thanks to Lagrange polynomial interpolation, the best pair of *ti* and *di* that most closely matches the PVGIS direct and diffuse value were found, doing therefore a local calibration. Using the Spline interpolation tool, these calibrated points were transformed into continuous monthly *ti/di* surfaces. Finally, the monthly maps of direct and diffuse radiation were generated by applying again Lagrange direct polynomial interpolation over the precomputed ArcGIS results, guided by the *ti/di* surfaces. This workflow, that is going to be explained better in the chapter 2, makes possible the consideration of actual atmospheric variability along with relief effects, reducing bias and maintaining the project's 2-meter resolution.

There are very few examples of the calculation of ET_o maps where solar irradiation is defined directly by using GIS tools, considering slope, aspect, and topographic shading.

Two remarkable studies were carried by Mészároš and Miklánek (2006) and Aguilar et al. (2010). Our workflow is based on those, but tries to go further by introducing a spatial, monthly calibration of ti and di against a distributed reference field (PVGIS). In addition, very high-resolution (2 m) products are generated, which incorporate topographic influences into Rn and consequently in ET_o , for more precise cultivation-suitability analyses.

1.4. Goals and attended results

- The production of monthly digital maps of direct and diffuse solar irradiation over inclined mountain surfaces, considering slope, aspect, and topographic shading starting from a 2 m DEM of the entire Aosta Valley. The spatial resolution of all the outputs regarding the solar radiation must be 2 m.
- The calibration of atmospheric parameters against PVGIS with the goal to use them to generate monthly R_s, and consequently, R_{so} and R_n, which are going to be used in raster algebra.
- The calculation of ET_o (FAO-56 Penman-Monteith) using net radiation mentioned above, maintaining high spatial resolution and giving the right importance at the topography. The results will consist in raster layers and statistics per parcel/zone for water balance and better manging of the plant.
- The creation of a suitability analysis for the herbaceous plant by combining the ET_o
 raster maps with topographic factors such as elevation, slope and aspect and with landuse information.
- The calculation of Crop Evapotranspiration of the existing cultivated fields for a month of specific interest of the A.U. life selecting a suitable crop coefficient from similar herbaceous plants. This permits the evaluation of the water deficit of each existing fields and of the area of agricultural interest in general.

2. Material

For this investigation, a collection of data was brought together with the intent of properly profiling the geographic setting and climatic factors impacting evapotranspiration:

- 1. The PVGIS datasets (Photovoltaic Geographical Information System) was used as the key origin of irradiation informations, offering both Global Horizontal Irradiance (GHI) as well as the proportion in between direct and diffuse components (Id/I). This data relies on the EUMETSAT CM SAF SARAH-3 satellite radiation data set for Europe.
 - Using a Python code, these two data sets were downloaded for each point on a grid, spaced 2 km apart, covering the entire Aosta Valley region. The available years downloaded are 19, from 2005 to 2023, from which an average year was then calculated. From these, direct and diffuse irradiation were calculated.
- 2. A 2 m resolution Digital Terrain Model (DTM) was used, to accurately capture the environment's features in the study area. Having this level of detail was very important to understand slopes, directions, and shadows, which all have a big impact on how much sunlight different spots receive. The downloaded DTMs were stitched together to create a smooth, high-resolution map of the entire studied area.
- 3. The minimum and maximum air temperature were obtained from ERA5, and they represent the year 2020. This kind of data cover the entire Europe with a 30-arc-second resolution.
 - The monthly mean was calculated starting from these daily fields and comparing the semi-sum of minimum and maximum temperature against the 2005–2023 PVGIS monthly mean temperatures. This brings up monthly anomalies, such as the increment of +2.1 °C of January 2020 compared to the mean of the same month from 2005–2023. The bias-correction were applied offsets to the monthly mean Tmax and Tmin models used in the FAO-56 ETo calculations. The original reference system of the temperature raster maps was WGS84, therefore were reprojected to UTM 32N, to create consistency with the rest of the workflow.
- 4. A shapefile containing the existing cultivated fields of the studied plant was provided from the Department of Agriculture of the region. This data is fundamental to compare the result obtained from the methodology and the actual conditions of the field, other than predict future useful locations where the growth of the plants would be successful.
- 5. Total precipitation data was downloaded with a Python code from ERA5–Land with a resolution of 9 km for a 30-year period from 1995 to 2004, in order to construct a mean monthly value of July in mm/day.

3. Methodology

3.1. Calibration and estimation of transmissivity and diffusivity coefficients

The transmissivity (*ti*) and diffusivity (*di*) coefficients were estimated through a process that blends data from PVGIS with simulations run in ArcGIS. The objective is to define spatially detailed coefficients that are going to be needed to create radiation models customized to the specific terrain features of the study area.

Starting from the average monthly values for horizontal, direct, and diffuse solar radiation from the PVGIS database at points arranged in a regular grid spaced every 2 km, 818 points covering the entire region, monthly simulations of horizontal solar radiation (covering both direct and diffuse components) at those same points in ArcGIS, have been run.

Different sets of transmissivity and diffusivity coefficients have been tested, keeping *di* equal to 0.5 and changing *ti* in 0.2, 0.4, 0.6, and 0.8. Although these values could theoretically range from 0 to 1, the 0.2 to 0.8 range was considered the most realistic in this scenario.

Keeping the diffusivity coefficient equal to 0.5 was fundamental in saving computational time. This was achieved thanks to the following reasoning that starts with the basic Formula (3) for diffuse radiation:

$$Dif\theta, a = Rglb \times Pdif \times Dur \times SkyGap\theta, a \times Weight\theta, a \times \cos(AngIn\theta, a)$$
 (3)

Here is possible to notice that diffuse radiation in a sector depends on:

- Rglb = normal global radiation
- *Pdif* = diffusivity coefficient, which is the fraction of global radiation that becomes diffuse.
- Geometric/temporal terms such as Duration factor (Dur), Sky view factor ($SkyGap\theta, a$), Directional weighting factor ($Weight\theta, a$), Cosine of incidence angle ($cos(AngIn\theta, a)$).

The Formula (4) of *Rglb* is:

$$Rglb = \frac{Sconst \sum \beta^{m(\theta)}}{(1 - Pdif)} \tag{4}$$

Where $\beta^{m(\theta)}$ is the Atmospheric transmittance function, Sconst is the solar constant and Pdif is the diffuse proportion.

Rglb has (1 - Pdif) in the denominator and therefore it is a function of transmissivity corrected by the fraction of direct radiation.

In conclusion, diffuse radiation turns out to be a function of transmissivity (included in βm (θ)) multiplied by a function of the diffusivity coefficient Pdif, as it is showed in the following Formula (5):

$$Dif\theta, a = \frac{(SConst \times \sum (\beta^{m(\theta)}))}{1 - Pdif} \times Pdif \times (Dur \times SkyGap\theta, a \times Weight\theta, a \times \cos(AngIn\theta, a))$$
 (5)

These two variables are separate, they do not "mix", so they can be treated independently in the calibration.

Special case happens when *Pdif* is equal to 0.5, showed in the Formula (6):

$$\frac{Pdif}{(1 - Pdif)} = \frac{0.5}{1 - 0.5} = 1\tag{6}$$

In practice, when *Pdif* is equal to 0.5, diffuse radiation depends only on transmissivity (ti) and geometric/temporal factors (duration, sky gap, angle, etc.).

The following step was the calibration of these coefficients using inverse polynomial interpolation. This meant comparing PVGIS radiation data with the values generated in ArcGIS for the same points of the 2-km grid to find the best transmissivity and diffusivity values for each point. This novel approach takes advantage of PVGIS as a reliable reference, making the coefficient estimation more accurate.

Once the monthly best pair of coefficients for transmissivity and diffusivity were obtained in every point, continuous maps of their spatial distribution were created using an interpolation method as explained in the chapter 3.2.2.

3.2. Spatial analysis and radiation modelling over agricultural area.

3.2.1. Delimitation of the potential agricultural area

To identify the potential agricultural area, the topographical information of the fields using the "zonal statistics as table" ArcGIS command was analysed. The tables show that:

- All fields are between an altitude of 1300 metres (1343) and 1800 (1786).
- The slope ranges from 0 to 45 (44.3) degrees.
- Regarding the aspect, there is a clear preference for southern exposures, particularly south and south-east. This distribution is compatible with the need to maximise solar radiation in a mountainous context. However, because some of the already present fields have an orientation of Nord and Nord-West too, aspect has not been considered in the selection of the area of interest, to do not exclude any of these already present fields.

Accordingly, with this information, raster with binary values (0 or 1) of altitude and slope were created to obtain the cells that satisfy both conditions, resulting in the green portion of the region (Figure 6), which in fact contains all the fields.

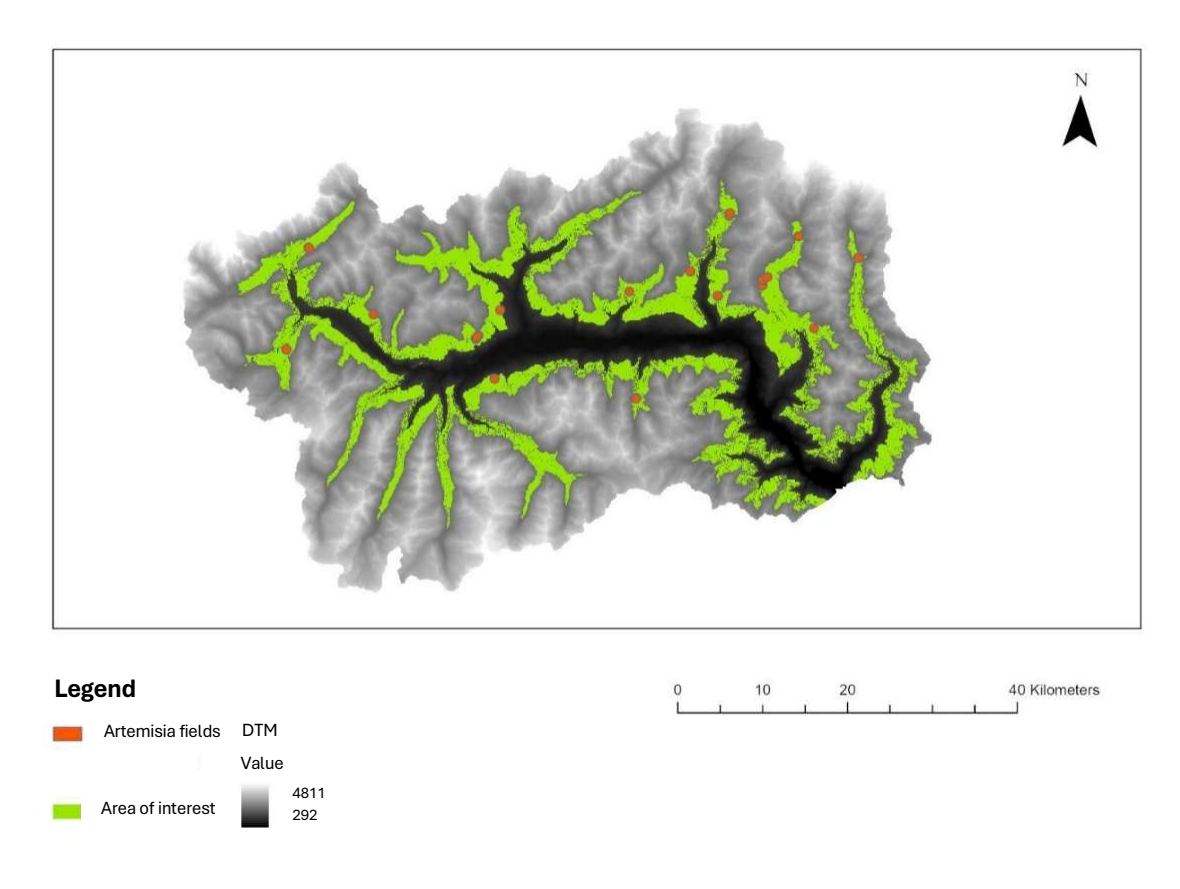


Figure 6. Area of agricultural interest (green), Artemisia umbelliformis fields (red).

3.2.2. Spatial interpolation of coefficients

From now on the methodology is going to be explained considering as example the month of January to show all the steps and results. The same methodology will be applied to analyse the month of July since the plant is in full bloom this month.

Comparison of interpolation methods using MRSE

To investigate the best interpolation method for spatially estimating the coefficients of transmissivity (*ti*) and diffusivity (*di*) calculated before, a systematic comparison was conducted between three commonly used techniques: Spline, Kriging and IDW. The object is to subsequently process the raster maps of these coefficients that were most closely related to the actual values processed by PVGIS, area solar radiation and Lagrange algorithm.

The focus was placed on the area of agricultural interest.

The dataset composed by the 2-km grid points of the area of interest, containing 146 reference points, was divided into 2 sub-datasets:

- a model interpolation set, which is the training data for building interpolation models.
- validation points used to test the accuracy of the results.

Every other point was selected to equally distribute the spatial look of each group (Figure 7)

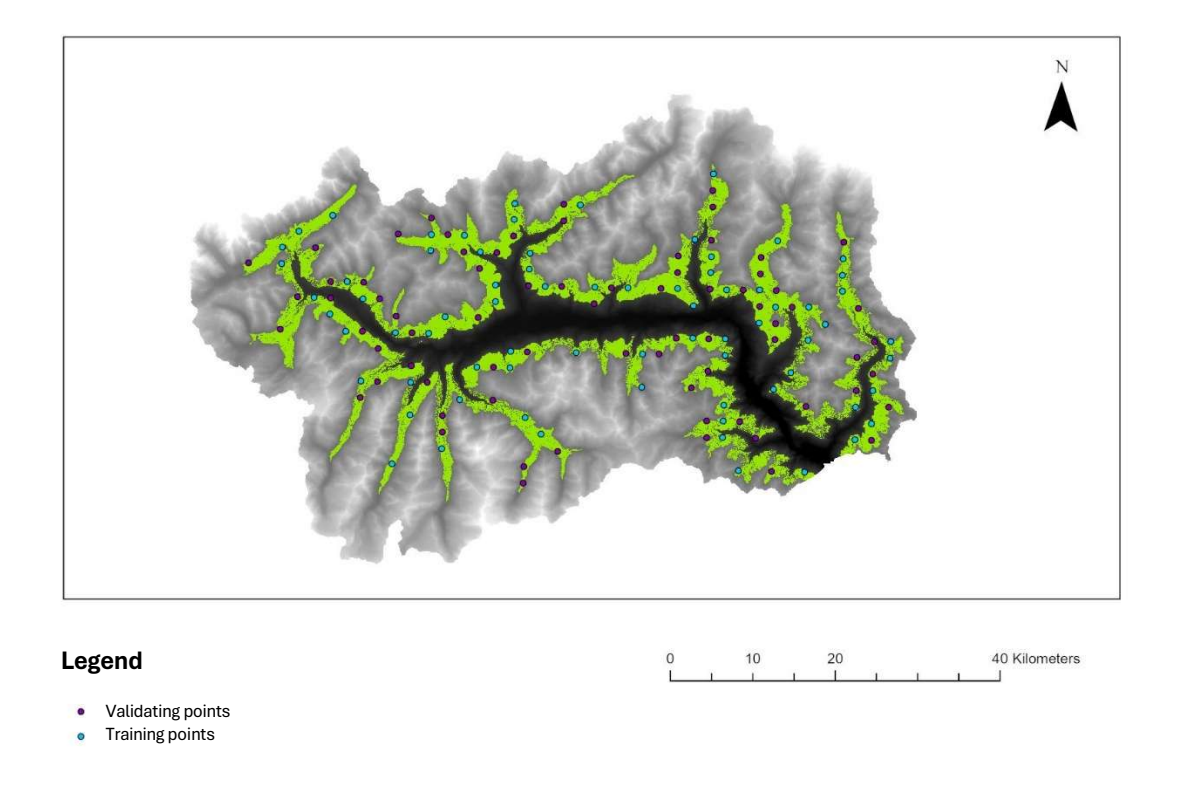


Figure 7. Training points (light blue), Validating points (purple).

An interpolated raster was created for each method, derived solely from the training points. Then the RMSE (root mean square error) method was used, to compare the values against the real output of selected validation points.

The process went through the following three main steps:

- 1. Interpolated values were extracted at the validation points using the "Extract Multi Values to Points" tool.
- 2. The quadratic difference between the actual value and each interpolated value was calculated.
- 3. Calculation of the mean of the quadratic errors, followed by the square root of the result, according to the Formula (7):

$$RMSE = \sqrt{\frac{1}{n} \sum_{i=1}^{n} (z_r - z_i)^2}$$
 (7)

Where:

 z_r is the real value.

z_i is the interpolation estimated value.

n is the total number of validation points.

This value provides a quantitative indication of the accuracy of the different methods: lower values indicate greater adherence to the real data.

For the method of Spline, three configurations were tested using different pairs of parameters which has been selected following some considerations (Table 1).

The "weight" parameter controls the rigidity of the interpolated surface. Lower values permit to follow more closely the local variations present in the data, higher values, instead, produce smoother surfaces. The values 0.1, 0.2 and 0.3 represent a limited range but are sufficient to test the effect of tension, as also suggested in the official ArcGIS documentation1. (ESRI. (2023). How Spline works. ArcGIS Pro Documentation)

The "number of points" parameter indicates the number of close that points are considered to calculate the interpolated value in each raster cell. Having 146 points distributed across the agricultural area of interest, values between 12 and 20 provide a good balance between local detail and spatial continuity.

Model	Weight	N. of points
SA	0.1	12
SB	0.2	16
SC	0.3	20

Table 1. Different spline parameters.

For the method of Kriging, different tests were conducted (Table 2) keeping the search radius fixed at 12 cells, to focus on the effect of the semi-variogram model. The curves tested such as Spherical, Exponential and Gaussian, are commonly adopted in spatial variation models.

The Ordinary Kriging Method was tested for the interpolation of the transmissivity and diffusivity coefficients as it is one of the most robust and theoretically justified estimation methods. Since the data wander from the continuum without showing a clear global trend, the assumption of a constant local mean was appropriate. Moreover, as ordinary Kriging is a BLUE

estimator, i.e. the best in terms of variance among linear and unbiased estimators, if the model conditions are met.

Table 2. Different Kriging parameters.

Model	Semi-variogram model	N. of points
KA	Spherical	12
KB	Gaussian	12
KC	Exponential	12

Also, the Inverse distance Weighting (IDW) was tested as an alternative interpolation method with a couple of different combination of parameters changing the number of points between 12 and 20.

Choosing the Optimal Method

Table 3. Comparison of the different methods.

Test	Mean squared error	Time of calculation
SA	0.0205	21 min
SB	0.0201	24 min
SC	0.0195	27 min
KA	0.0223	6 h 13 min
KB	0.0273	7h 10 min
KC	0.0205	8 h 15 min
IDWA	0.0220	13 min
IDWB	0.0224	17 min

Knowing all the mean square errors show that the smallest one is the one obtained with the third configuration of Spline (Table 3). Since for the method of Spline the combination of "weight" 0.3 and "number of points" 20 gave the best results, other tests were carried keeping constant the value of the weight at 0.3 and changing the number of points to 12, obtaining a quadratic error of 0.02042, and to 16 obtaining a quadratic error of 0,0196 which confirms that for spline the best parameter for the number of points is 20.

Among all the interpolation methods tested, the Spline method was the most effective for the spatial estimation of the transmissivity (*ti*) and diffusivity (*di*) coefficients. The Spline approach works well in minimizing surface curvature and produces smoother and continuous fields, a highly desirable feature when modelling atmosphere variables, which change gradually in space. While IDW resulted in circular artifacts ("bull's-eye effect") and exaggerated local differences, Spline interpolation preserved spatial gradients that were more realistic and consistent with the physical behavior of transmissivity over the mountainous terrain.

On a theoretical level, Kriging is quite powerful, however, the accuracy is not higher (best of Kriging 0.0205 versus best of Spline 0.0195). Moreover, given the regular and dense sampling

of PVGIS grid points in this study, the computational expense and significant variogram fitting required by Kriging does not appear to be justified.

Considering all these factors, the Spline method achieved the best trade-off between accuracy, computational efficiency, and physical consistency. It was then used to generate the monthly transmissivity and diffusivity surfaces.

Similar findings have also been reported in literature. According to Li and Heap (2014), spline methods, in particular thin-plate and regularized spline interpolators, are found to be most effective in the case of smooth and continuous environmental variables like temperature, precipitation, or radiation. This effectiveness is especially pronounced when the sampling points are dense and evenly distributed. The cited reference thus provides a rationale for selecting the Spline method to obtain spatial patterns of transmissivity and diffusivity coefficients that are physically consistent in this research.

Finally, Spline interpolation for *ti* (Figure 8) using all the points of the area of agricultural interest:

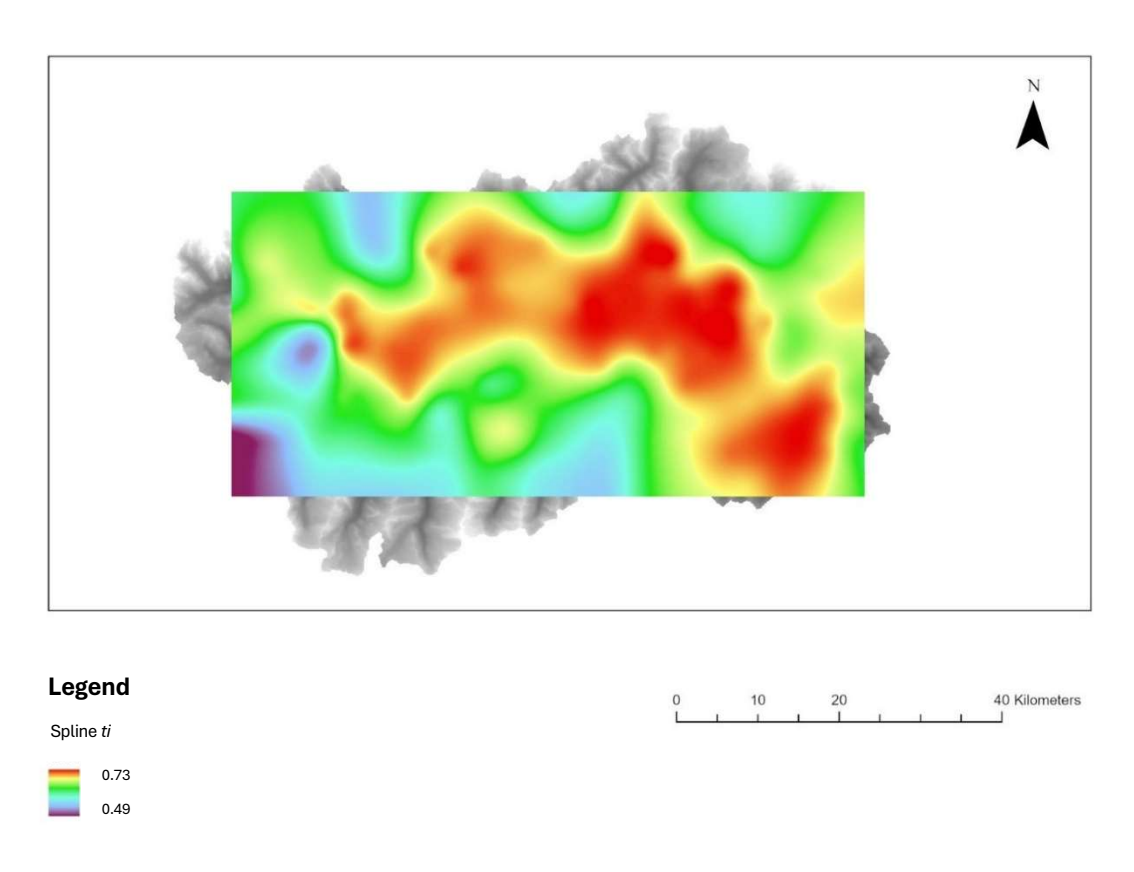


Figure 8. Visual representation of ti interpolation in the agricultural area.

The same interpolation has been applied to *di* values.

3.2.3. Real radiation maps over agricultural area

Using the command "raster solar radiation" on ArcGIS, monthly digital models of solar radiation (direct and diffuse) for pre-established values of transmissivity (0.2, 0.4, 0.6 and 0.8) and diffusion (0.5) coefficients were created, considering not only the altitude but also the orientation, slope and surrounding relief of each pixel (Figure 9).

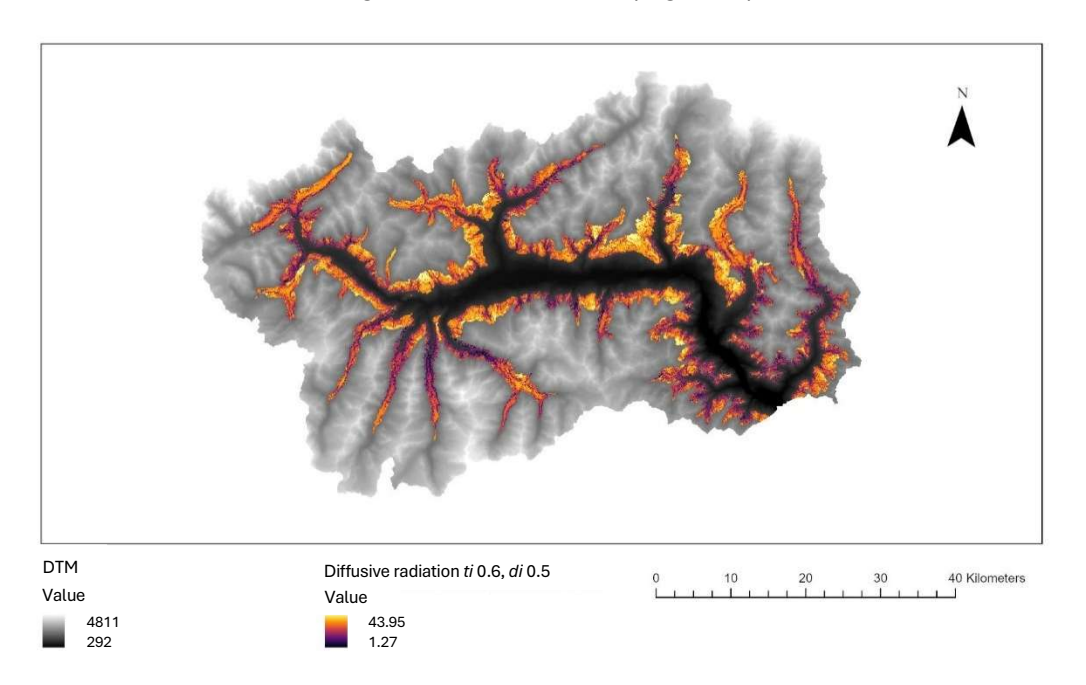


Figure 9. Visual example of January diffuse radiation with transmissivity coefficient 0.6 and diffusivity coefficient 0.5 [kWh/m²].

Because of the long calculation time and of the weight in the meaning of space occupation of all these maps, the project will consider, whenever it is possible, only the area of agricultural interest (Figure 6).

For each month, using direct polynomial interpolation with the ArcGIS raster calculator, the final monthly digital models of direct (Figure 10) and diffuse irradiation (Figure 11) were created, using the digital models of transmissivity and diffusivity coefficients generated with Spline interpolation in the chapter before. This process follows three Formulas (8), (9), (10). For direct irradiation:

$$B = \frac{(t_p - t_2) \times (t_p - t_3)}{(t_1 - t_2) \times (t_1 - t_3)} \times B_1 + \frac{(t_p - t_1) \times (t_p - t_3)}{(t_2 - t_1) \times (t_2 - t_3)} \times B_2 + \frac{(t_p - t_1) \times (t_p - t_2)}{(t_3 - t_1) \times (t_3 - t_2)} \times B_3$$
(8)

Where:

t_p: transmissivity coefficient map obtained with Spline interpolation.

t₁: 0.2 for the months from April to September and 0.4 for the months from October to March.

t₂: 0.4 for the months from April to September and 0.6 for the months from October to March.

t₃: 0.6 for the months from April to September and 0.8 for the months from October to March.

B₁: direct irradiation map for the transmissivity value of 0.4 for January.

B₂: direct irradiation map for the transmissivity value of 0.6 for January.

B₃: direct irradiation map for the transmissivity value of 0.8 for January.

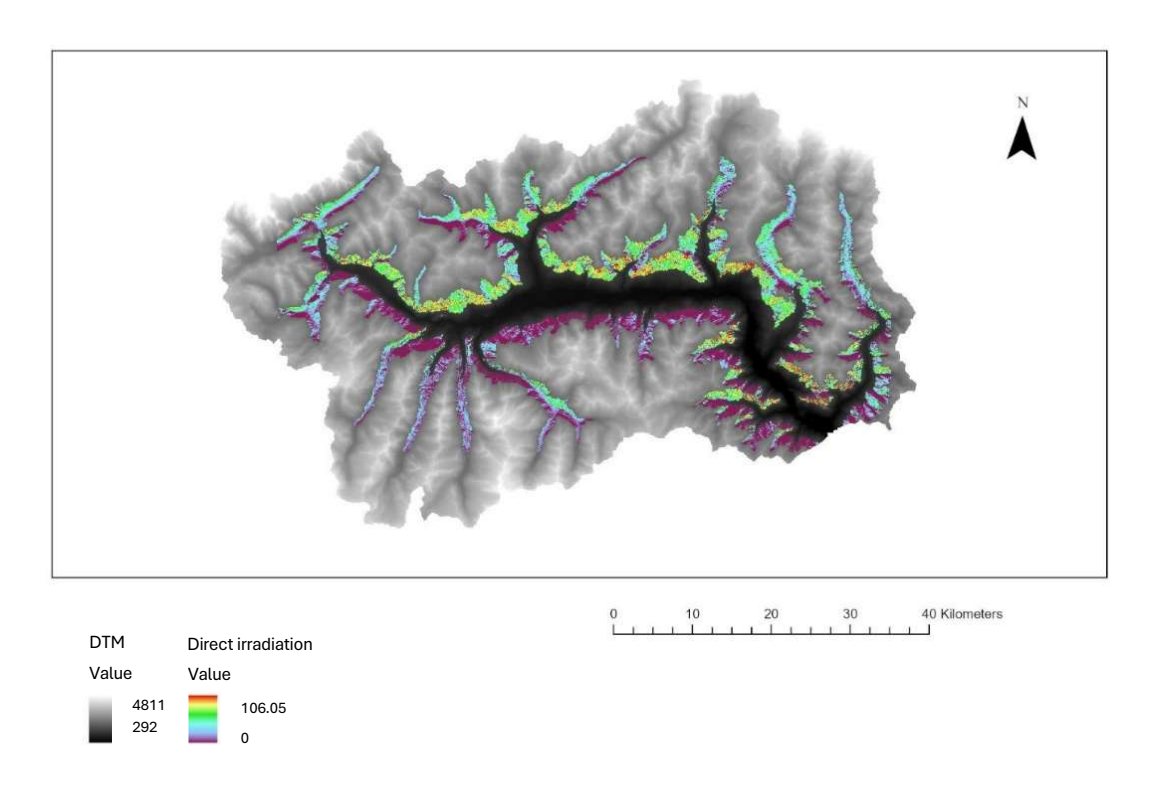


Figure 10. Direct irradiation [kWh/m²]

For the diffuse irradiation:

$$D = D_{0.5} \times (\frac{d_p}{1 - d_p}) \tag{9}$$

 d_p : diffusivity coefficient map obtained with the spline interpolation.

$$D_{0.5} = \frac{(t_p - t_2) \times (t_p - t_3)}{(t_1 - t_2) \times (t_1 - t_3)} \times D_1 + \frac{(t_p - t_1) \times (t_p - t_3)}{(t_2 - t_1) \times (t_2 - t_3)} \times D_2 + \frac{(t_p - t_1) \times (t_p - t_2)}{(t_3 - t_1) \times (t_3 - t_2)} \times D_3$$
(10)

Where:

t_p: transmissivity coefficient map obtained with Spline interpolation.

t₁: 0.2 for the months from April to September and 0.4 for the months from October to March.

t₂: 0.4 for the months from April to September and 0.6 for the months from October to March.

t₃: 0.6 for the months from April to September and 0.8 for the months from October to March.

D₁: diffuse irradiation map for the transmissivity value of 0.4 for January.

D₂: diffuse irradiation map for the transmissivity value of 0.6 for January.

D₃: diffuse irradiation map for the transmissivity value of 0.8 for January.

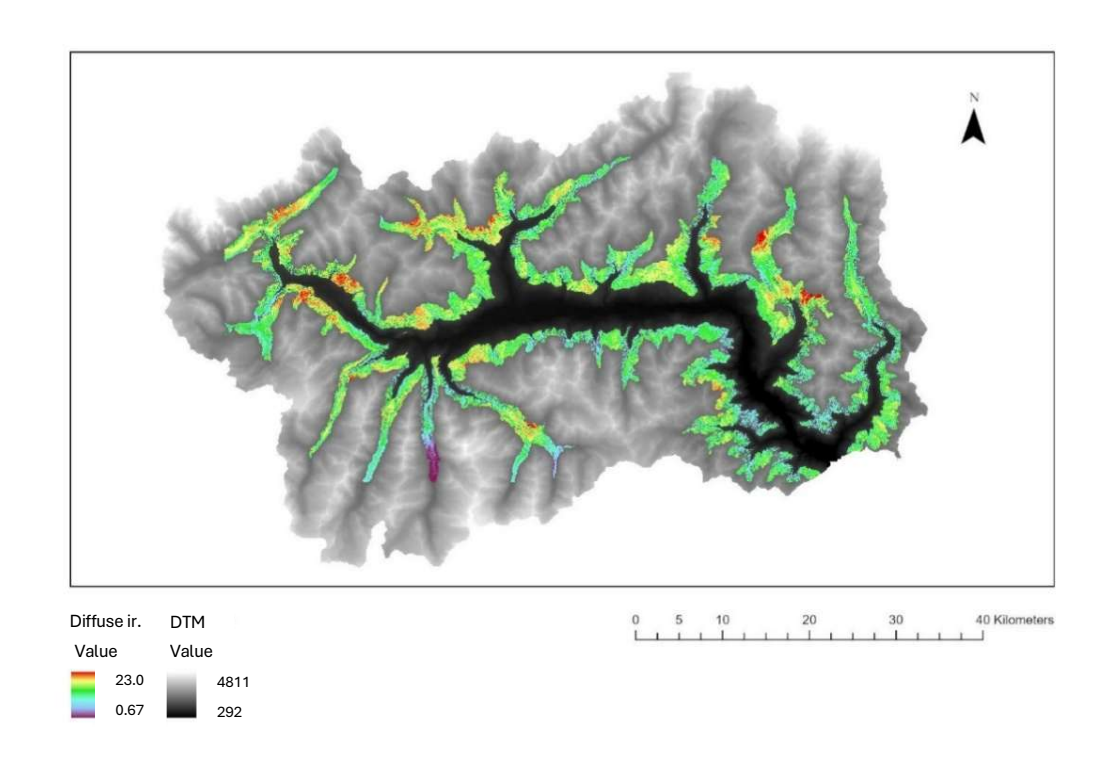


Figure 11. Diffuse irradiation [kWh/m²]

With the sum of direct and diffuse irradiation the global radiation was obtained (Figure 12).

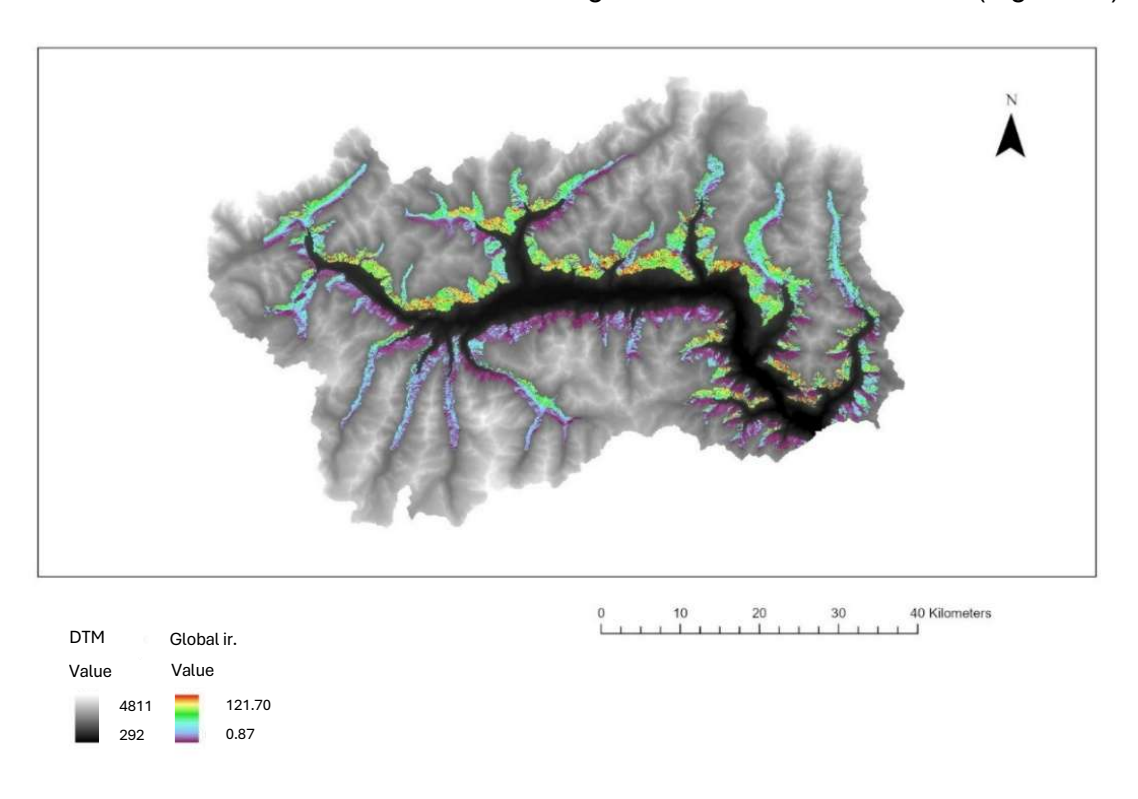


Figure 12. Global irradiation [kWh/m²]

Important correction

"Raster solar radiation" delivers energy for m² of sloped surface area. ET_o (FAO-56) requires radiation on a horizontal reference surface (typical for crops). According to Lambert's law (Formula 11):

$$Rs_horizontal = Rs_inclined / cos(\theta)$$
 (11)

On a slope ($\theta > 0$), the value of solar radiation per m² of horizontal ground is greater than the value per m² of inclined ground, because the same energy is 'concentrated' in a smaller projected area.

This correction prevents underestimating water and energy requirements per unit of horizontal soil

3.3. Calculation of potential evapotranspiration (ET_o)

The Penman-Monteith FAO equation was select to calculate ET_o , because as said before it is the most physically reliable and based empirical method. This method requires several meteorological parameters including T_{max} , T_{min} , R_s , relative humidity (calculated using the saturation vapour pressure equation e_s and e_a), wind speed (u_2) , atmospheric pressure (P), psychrometric constant (γ) , slope of the vapour saturation pressure curve (Δ) , net radiation (R_n) and ground heat (G), here considered negligible $(G \approx 0)$.

3.3.1. Calculation of all the parameters needed in the final formula

Mean temperature

Starting from the maps of minimum (Figure 13) and maximum (Figure 14) temperature, the calculation of the mean temperature (Figure 15) is made with the following Formula (12):

$$Tmean = \frac{(Tmax + Tmin)}{2} \tag{12}$$

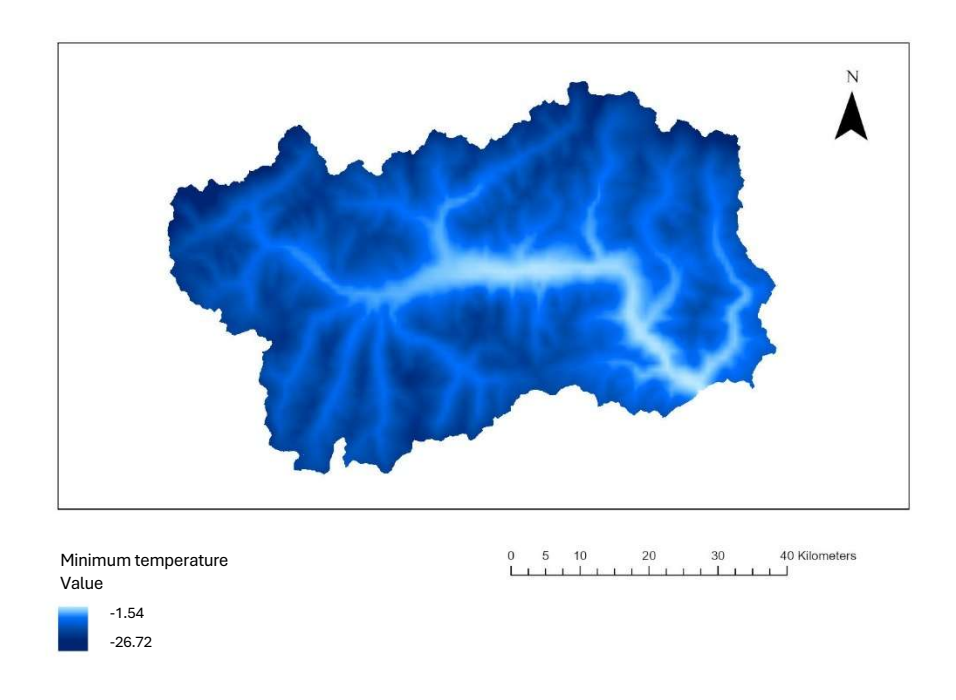


Figure 13. Visual representation of the minimum temperature of January [°C].

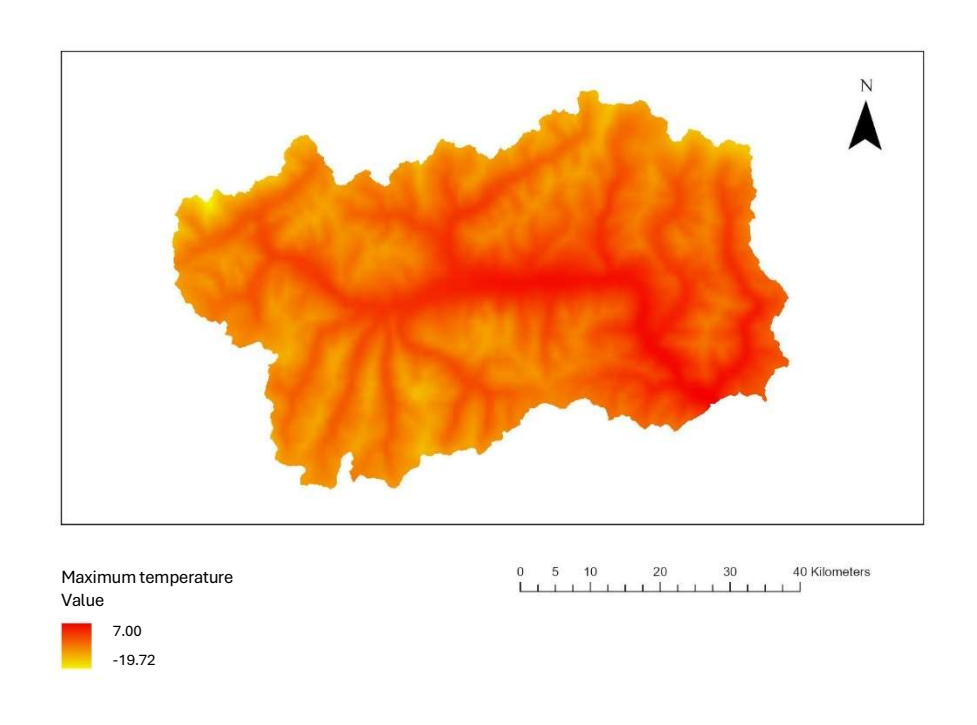


Figure 14. Visual representation of the maximum temperature of January [°C].

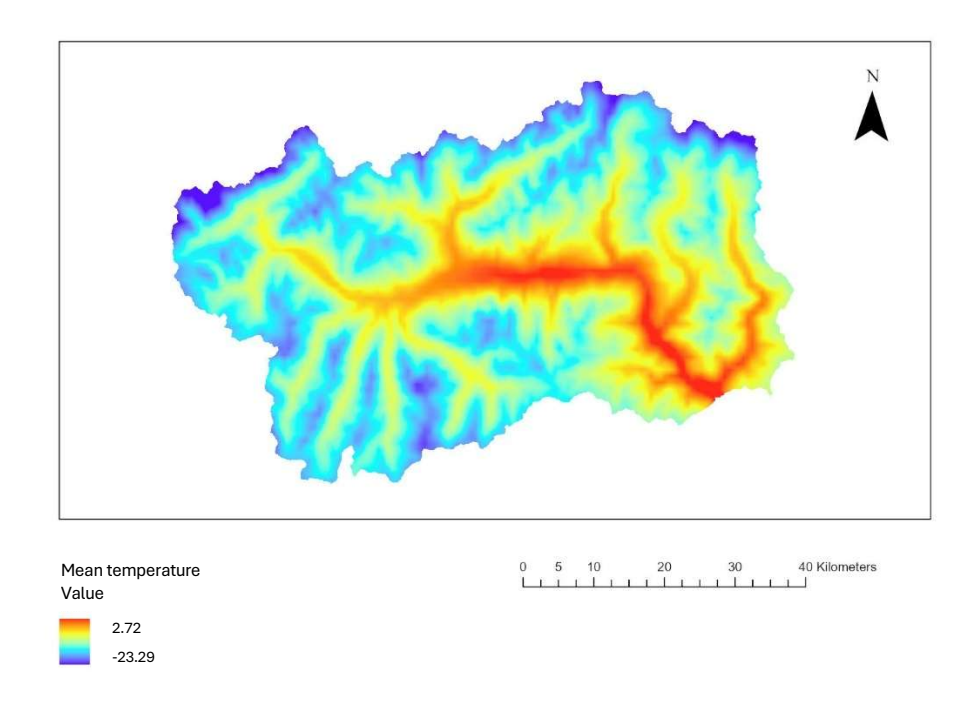


Figure 15. Visual representation of the mean temperature of January [°C].

Global radiation Rs

 R_s (Figure 16) is the sum of direct and diffuse radiation. The sum has been transformed from kWh/m^2 to MJ/m^2 and has been divided for 31 (number of days of January) to obtain the average daily irradiation obtaining values between 0.1 and 14.13. Since the radiation model already accounts for slope and orientation, no further correction for topography was necessary. The R_s map was also divided for the cosine of the slope (expressed in radians) as explained in the chapter 3.2.3.

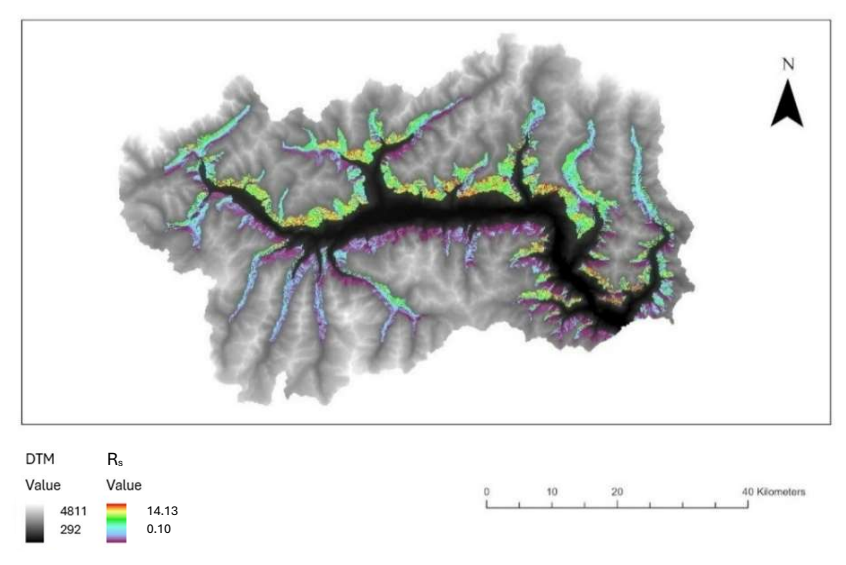


Figure 16. Visual representation of R_s [MJ/m²day]

Net shortwave radiation R_{ns}

This quantity (Figure 17) is calculated by (13):

$$R_{ns} = (1 - \alpha) \cdot R_s \tag{13}$$

where α =0.23 which is the medium albedo for herbaceous cultivations in absence of further data.

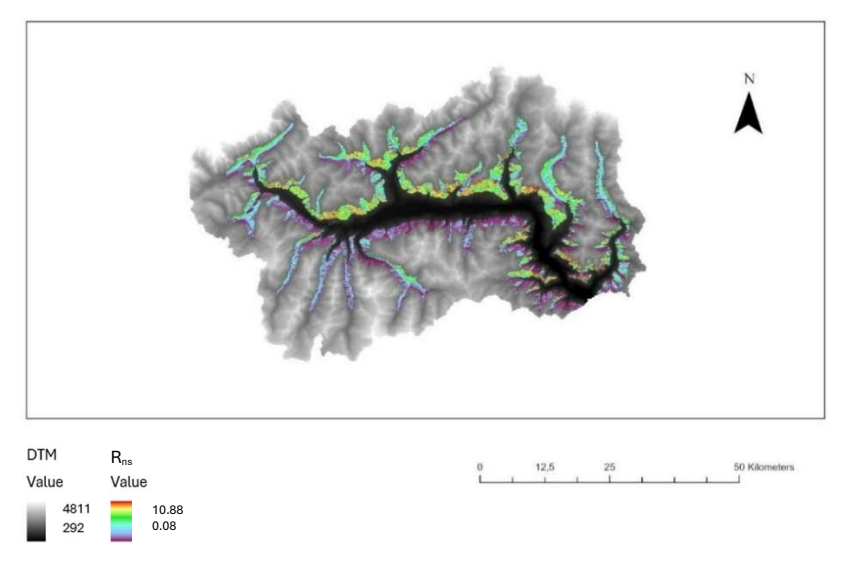


Figure 17. Visual representation of R_{ns} [MJ/m²day].

Irradiation in clear sky conditions R_{so}

To find the irradiation in clear sky conditions an option would be using the following formula given in the FAO literature (14):

$$R_{so} = (0.75 + ((2 * 10^{-5}) * DTM.tif) * R_a)$$
 (14)

Where R_a is the extraterrestrial solar radiation and is equal to 11.9 from literature table.

The result is the irradiation in clear sky conditions without considering the surrounding topography such as aspect and slope. The following step would be division of R_s for R_{so} just obtained. This creates an incongruence. R_s has been obtained through raster solar radiation considering all the topography effects, while R_{so} has been calculated in plane conditions.

Because obtaining another R_s in plane conditions is really time consuming at such high resolution, R_s/R_{so} has been approximated to D_{0.5} divided the diffuse radiation obtained with "raster solar radiation" with the highest value available of transmissivity coefficient, since it is directly proportional.

Net longwave radiation R_{nl}

The longwave radiation is obtained thanks to the Formula (15):

$$R_{nl} = 4.903 * 10^{-9} * \frac{((T_{max} + 273.16)^4 + (T_{min} + 273.16)^4)}{2} * (0.34 - 0.14 * \sqrt{e_a})$$

$$* (1.35 * \frac{R_s}{R_{so}} - 0.35)$$
(15)

Net radiation of the reference surface R_n

This quantity is given by the subtraction of the longwave radiation from the shortwave radiation.

Vapour saturation pressure es

$$e_{smax} = 0.6108 * Exp[17.27 * \frac{T_{max}}{(T_{max} + 237.3)}]$$
 (16)

$$e_{smax} = 0.6108 * Exp[17.27 * $\frac{T_{max}}{(T_{max} + 237.3)}]$

$$e_{smin} = 0.6108 * Exp[17.27 * $\frac{T_{min}}{(T_{min} + 237.3)}]$
(16)$$$$

e_{smin}: from 0.07 to 0.55

e_{smax}: from 0.13 to 1.02.

$$e_s = \frac{(e_{smax} + e_{smin})}{2} \tag{18}$$

E_s (Figure 18) grows exponentially with temperature, and it is obtained thank to the Formulas above (16), (17), (18).

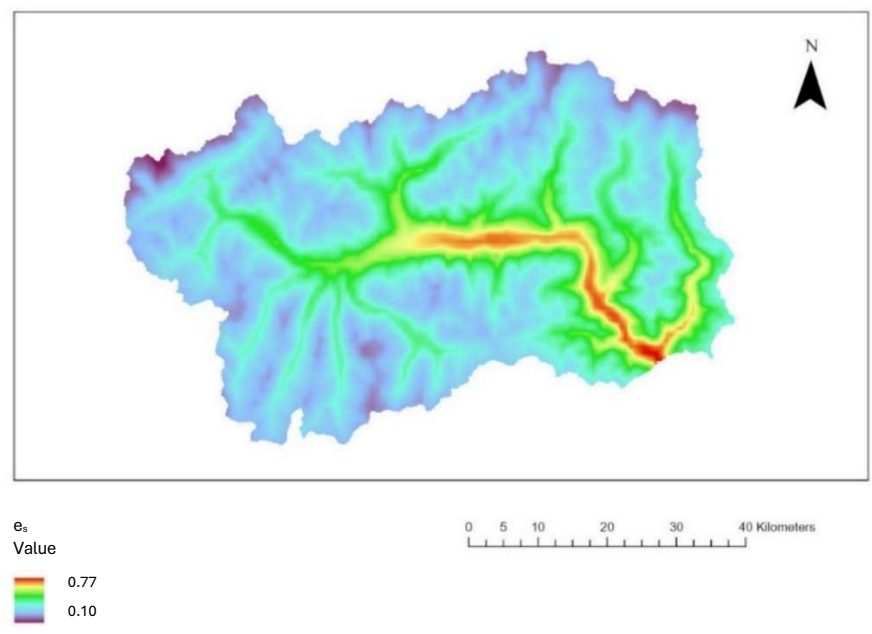


Figure 18. Visual representation of es [kPa].

Actual vapor pressure ea

Used to determine the vapor pressure deficit which drives the evaporative demand.

Bigger values of vapor pressure deficit mean a stronger evaporative demand. ea (Figure 19) is obtained thank to the Formula (19):

$$e_a = 0.6108 * Exp(17.27 * T_{min} / (T_{min} + 237.3))$$
 (19)

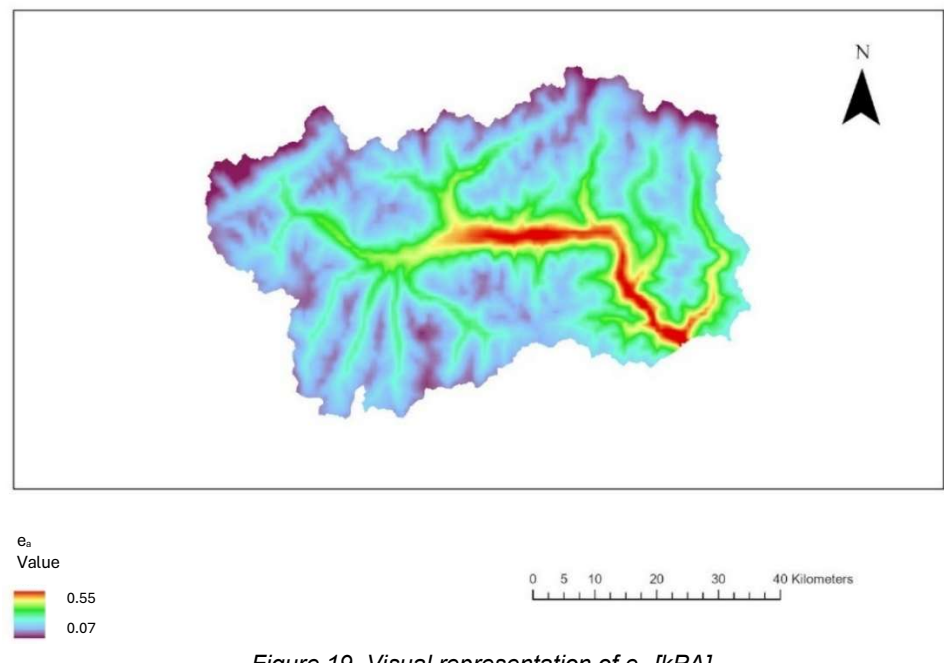


Figure 19. Visual representation of ea [kPA]

Wind velocity u₂

u₂ is approximated to 2 m/s if there are no further data.

Soil heat flux density G

G represents the rate of heat storage or release from the soil surface, measured in $MJm^{-2}day^{-1}$. For daily or monthly ET_o is assumed to be 0.

Stefan-Boltzmann Constant σ

It is a physical constant used to calculate longwave radiation emitted by a surface based on its absolute temperature, following the literature is equal to:

$$\sigma = 4.903 \times 10-9$$

Slope of the saturation vapor pressure curve Δ Obtained with the Formula (20):

$$\Delta = 4098 * \left(\frac{0.6108 * e^{[17.27 * T_{mean} / (T_{mean} + 237.3)]}}{(T_{mean} + 237.3)^2}\right)$$
 (20)

The result is between 0,008 and 0,052.

Pressure P

To obtain the pression map (Figure 20) the Formula (21) was followed:

$$P = 101.3 * \left(1 - \frac{0.0065 * DTM}{293}\right)^{5.26}$$
 (21)

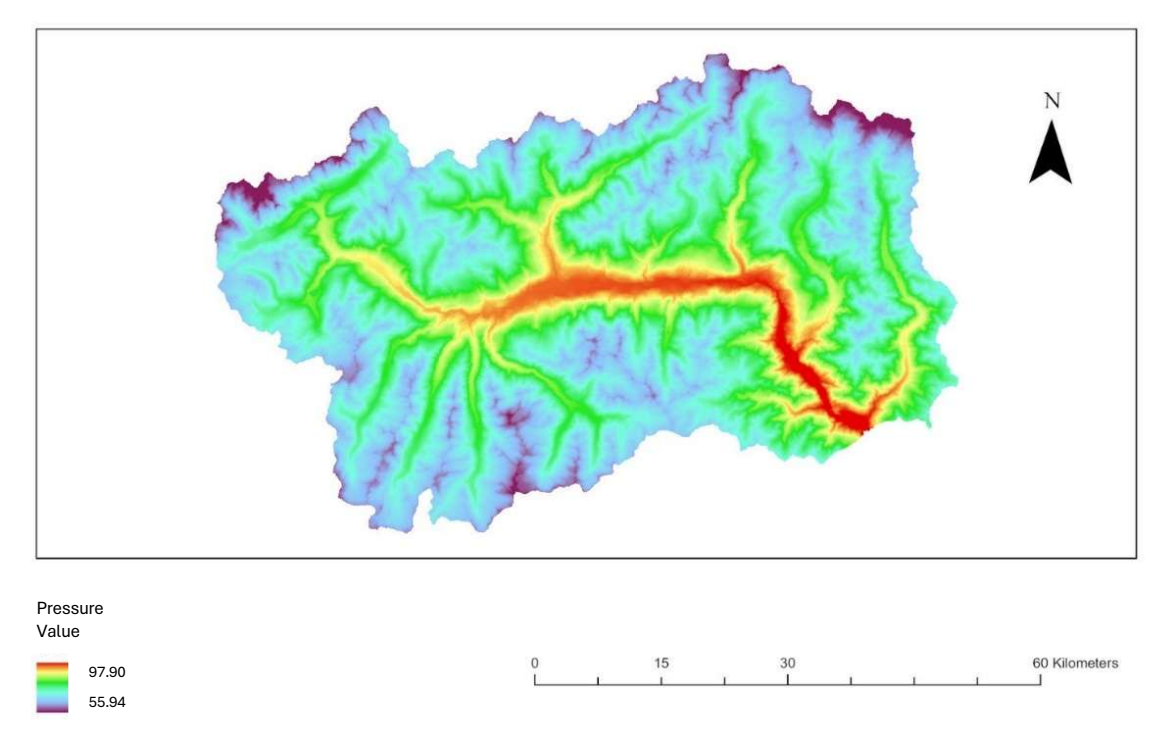


Figure 20. Visual representation of Pressure P [kPa].

Psychrometric Constant γ

$$\gamma = 0.000665 * P \tag{22}$$

These values obtained with the Formula (22) range between 0.037 and 0.065 and weights the aerodynamic component in the calculation of evapotranspiration.

The higher the atmospheric pressure (i.e. at low altitudes), the higher γ .

ET_o

Finally having all the parameters ready, is possible to execute the last Formula (23) in Raster Calculator:

$$ET_o = \frac{0.408 * \Delta * (R_n - G) + \gamma * \frac{900}{(T_{mean} + 273)} * u_2 * (e_s - e_a)}{\Delta + \gamma * (1 + 0.34 * u_2)}$$
(23)

4. Results

Histogram of January's Irradiation (Figure 21) of all the study area: min 0.26, max 19.30, mean 5.90 [MJ/m²day].

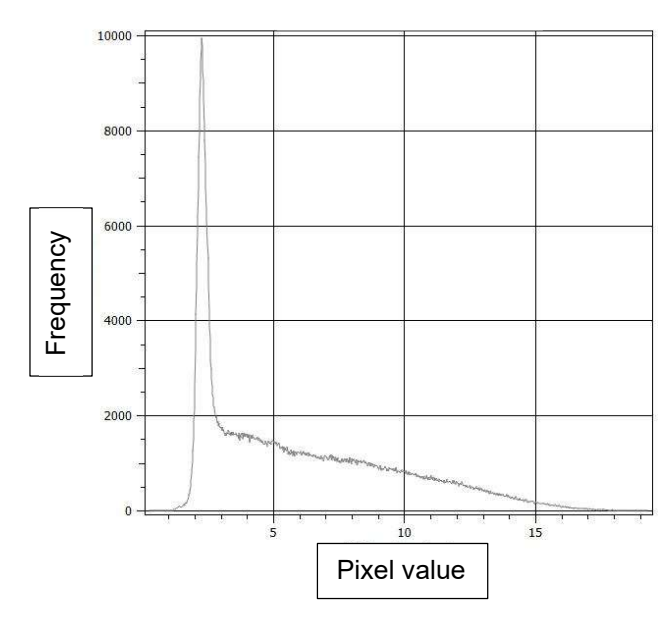


Figure 21. Histogram of the irradiation of the study area during January.

Overlapping this result with the Artemisia fields, the irradiation values present in the surface of the fields vary from a minimum of 3.39 to a maximum of 16.64, with an average of 9.28 [MJ/m²day].

The figures belove illustrate the reference evapotranspiration in the area of agricultural interest (Figure 22) and the corresponding histogram (Figure 23): min 0, max 1.39, mean 0.29 [mm/day].

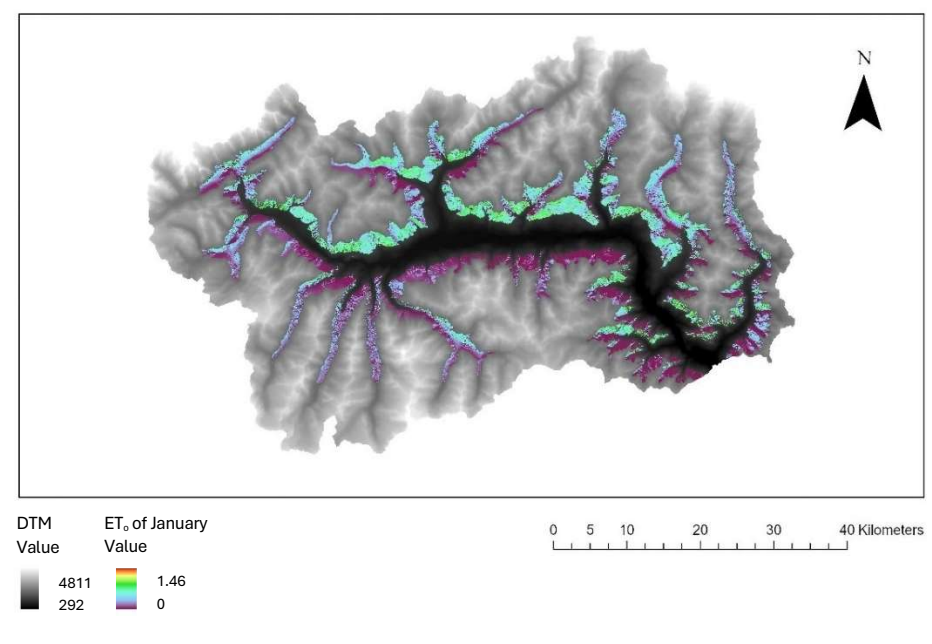


Figure 22. January's reference evapotranspiration [mm/day]

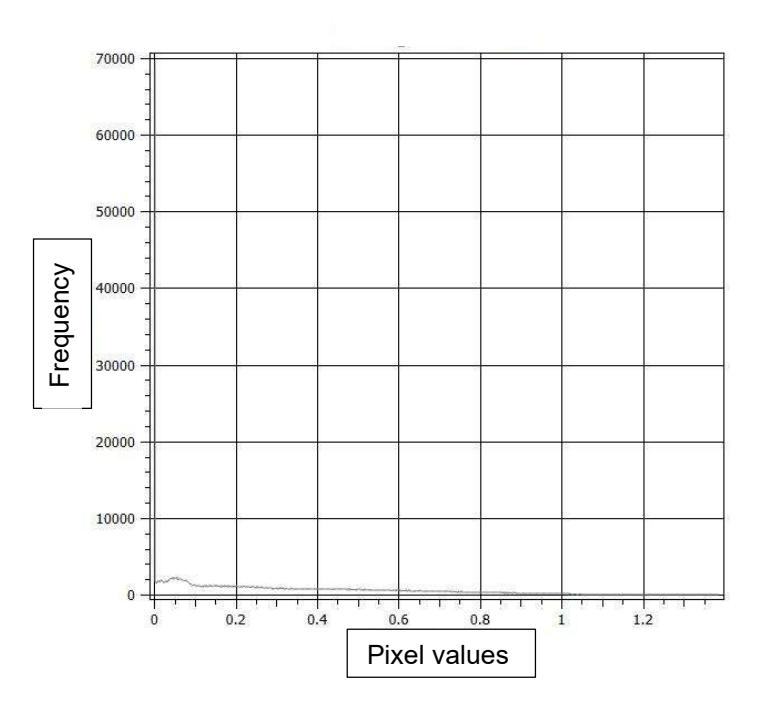


Figure 23. Histogram of January's Reference Evapotranspiration.

In the fields surface, the reference evapotranspiration values vary from a minimum of 0.14 to a maximum of 1.04, with an average of 0.54 mm/day.

The January results show that in the depths of winter, A.U. fields receive more solar energy and have an evapotranspiration demand that is almost double the average for the territory. This indicates favourable exposure and microclimatic conditions.

4.1. July's results

The same methodology has been applied to the month of July obtaining this value of irradiation (Figure 24) with the consequent histogram (Figure 25): min 0.93, max 33.38, mean 23.17 [MJ/(m²day)].

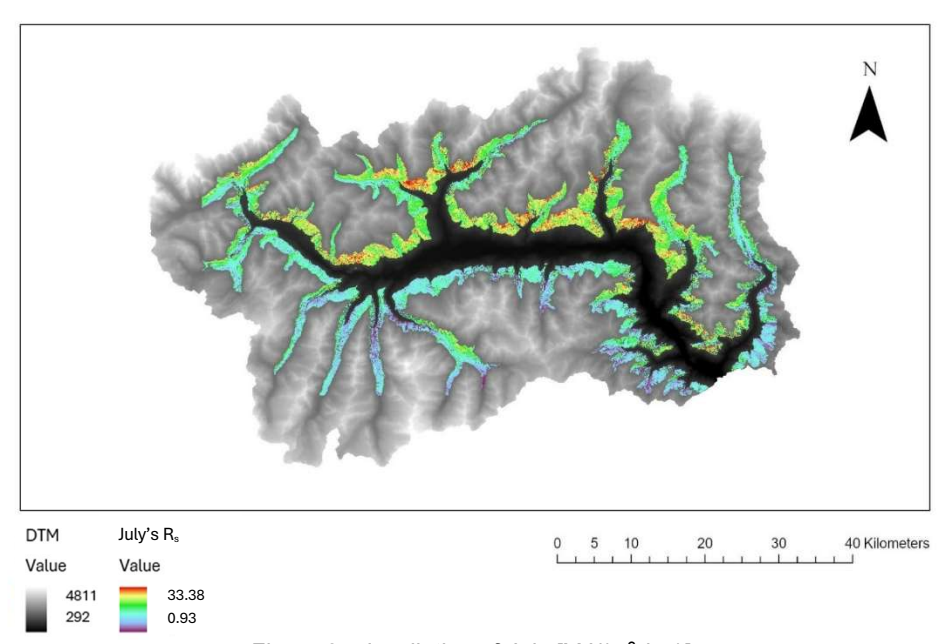


Figure 24. Irradiation of July [MJ/(m²day)]

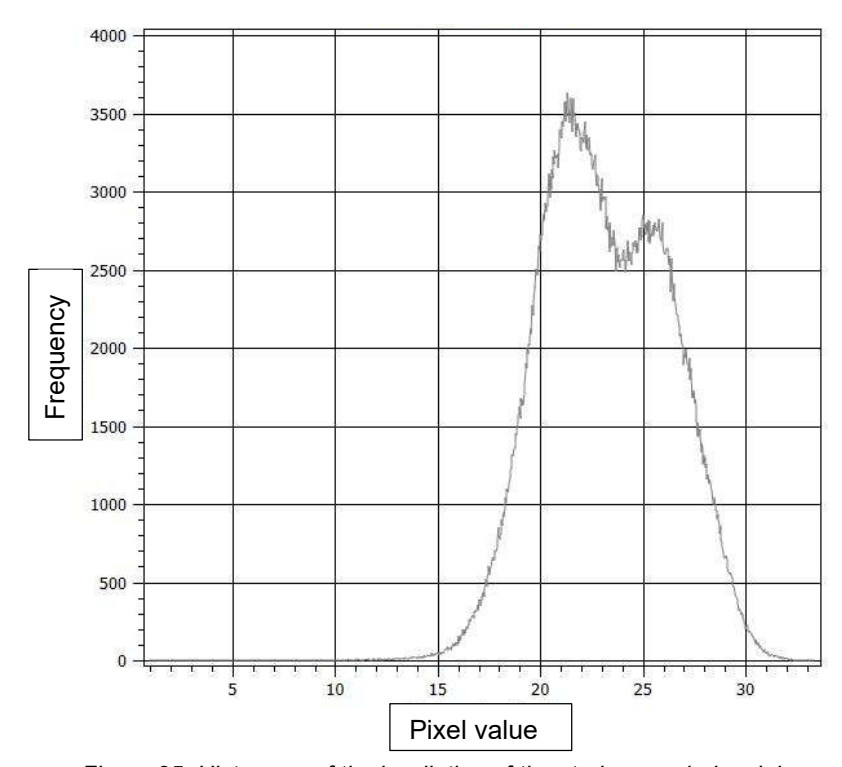


Figure 25. Histogram of the irradiation of the study area during July.

Overlapping this result with the *Artemisia umbelliformis* fields, the irradiation values present in the surface of the fields vary from a minimum of 18,72 to a maximum 29,52, with an average of 25,92 [MJ/(m²day)].

Regarding evapotranspiration in the totality of the study area (Figure 26 and 27): min 0.31, max 5.82, mean 4.12 [mm/day] .

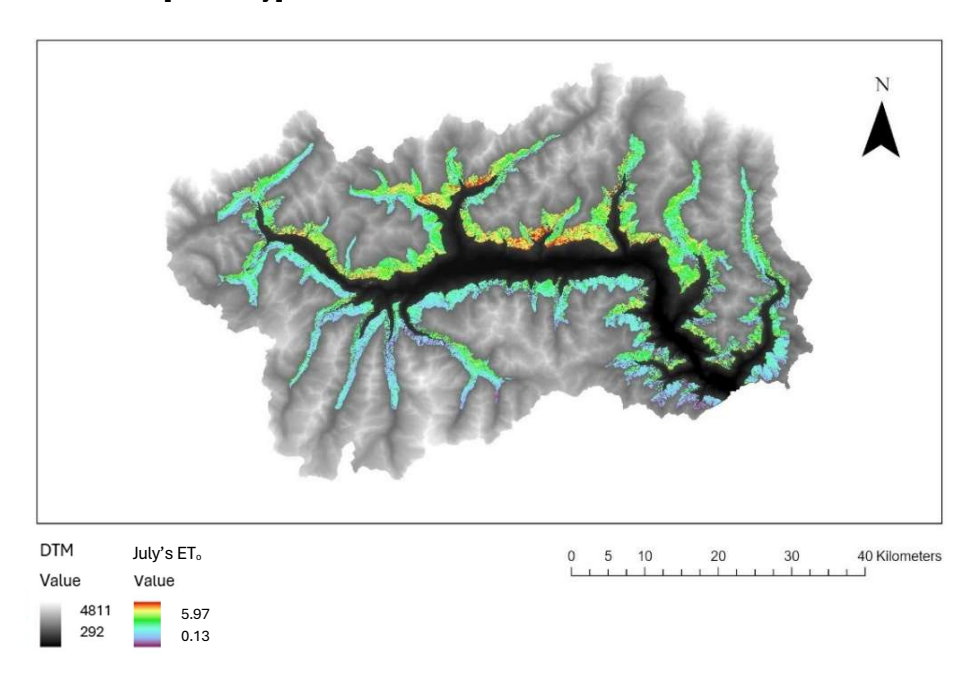


Figure 26. July's Reference Evapotranspiration [mm/day]

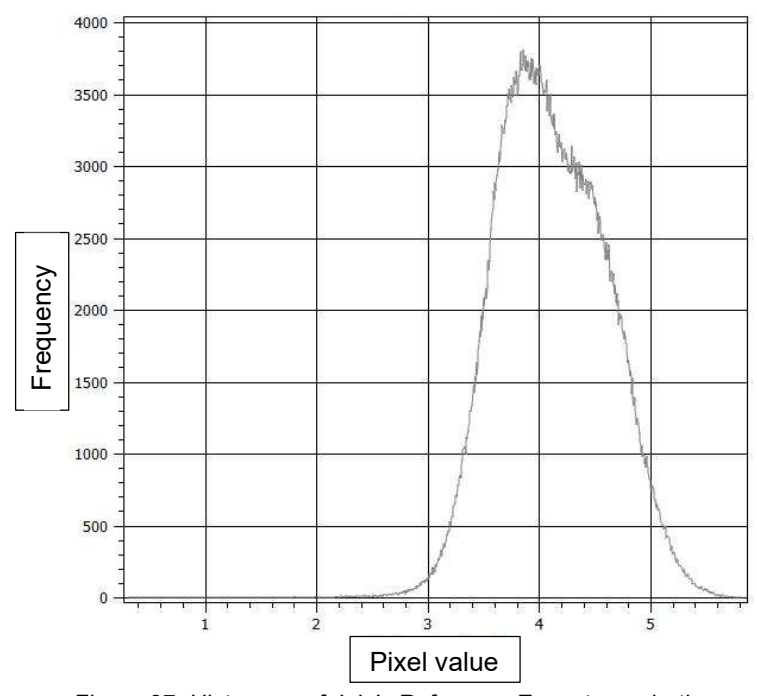


Figure 27. Histogram of July's Reference Evapotranspiration.

Considering all the 70 artemisia A.U. fields, with a median size of 26.5 cells of 2 meters, i.e. an area of $106~\text{m}^2$, the mean values of ET $_{\text{o}}$ range from 3.67 to 5.22 mm/day, with an overall mean 4.50 mm/day.

In summer, A.U. field values of ET_o and R_s remain higher compared to the total area, but the difference is less pronounced than in winter.

Therefore, Artemisia umbelliformis fields are ideal micro-areas.

5. Kc calculation

With the goal of obtaining the crop evapotranspiration (ET_c) raster, the identification of a proper crop coefficient (K_c) is needed. Since in January the plant is considered dormant, this part of the project is going to be focused only on the month of July, flowering period of A.U..

Since there is no direct FAO K_c for this plant, an approach based on physiological and morphological similarities with low-growing perennial aromatic herbs (sage, thyme and *Artemisia absinthium*) (Table 4) and on the FAO-56 guidelines for low herbaceous crops was adopted, analysing the similarities between the following plants:

Plant	Typology	Barrel height	Biological form	Flowering	Family
Artemisia umbelliformis	Herbaceous perennial, woody roots	20-30 cm	camefita fruticosa (Ch frut)	July- September	Asteraceae
Sage	Herbaceous perennial, woody at the base	20-40 cm	camefita suffruticosa (Ch suffr)	March-July	Lamiaceae
Thyme	Aromatic perennial, evergreen, coniferous	10-30 cm	camefita fruticosa (Ch frut)	<u>May-</u> <u>August</u>	Lamiaceae
Artemisia absinthium	Perennials and woody plants at the base base	0.5-1.5 m	camefita suffruticosa (<i>Ch suffr</i>)	July- August	Asteraceae

Table 4. Comparison between perennial aromatic herbs.

The establish K_c for the different phase of the plant's growth are (Table 5):

Plant	K _{cin}	K _{cmid}	K _{cend}
Artemisia absinthium (wormwood)	0.45	0.80	0.40
Salvia officinalis (sage)	0.30	1	0.45
Thymus vulgaris (thyme)	0.30	0.95	0.80

Table 5. Crop coefficients.

Rosmery and thyme are short, aromatic herbs, often non-irrigated or wild while *Artemisia absinthium* (wormwood) has same genus, similar "short herb/subshrub" architecture.

The month of July represent the period in which the A.U. is creating all its flower which are almost ready to be picked up. For this reason the K_{cmid} is the right coefficient that must be analysed for this month.

Starting from the standard values of *Artemisia absinthium*, its coefficient is adjusted to local climate and canopy traits (height, cover).

Using the formula (24) explained in FAO-56 Chapter 6 climate adjustment for single K_c:

$$K_{cmid} = K_{cmid}(tab) + (0.04 \times (u_2 - 2) - 0.004 \times (RH_{min} - 45)) \times (\frac{h}{3})^{0.3}$$
 (24)

Where RH_{min} is the minimum relative humidity (%) recorded in a day (or averaged over the period/stage) and u_2 is the wind velocity at 2 meters above the ground.

Ideally, the RH_{min} value can be obtained from weather stations.

For July in Aosta Valley RH_{min} is equal to 59% while the average wind at 10 m is equal to 13.5 km/h, converted to 2.81 m/s at two meters above ground.

h is the average height of the crop (in metres) during the stage considered; it represents the aerodynamic roughness of the canopy, typical for A.U. is equal to 0.5–0.20 m at full cover.

Correction applied to K_{cmid} =0,80 (Table 6) using the formula above (24) and the estimated value of wind and RH_{min} :

Table 6. Correction of K_{cmid}.

h (m)	July (59%, u ₂ = 2.81)	Δ
0,15	0.790	-0.027
0,20	0.790	-0.029

Correction applied to K_{cmid} =0,80 (Table 7) considering instead the wind velocity at 2 m/s as suggests FAO manual:

Table 7. Correction of K_{cmid} with standard wind velocity.

h (m)	July (59%)	Δ
0,15	0.777	+0.008
0,20	0.775	+0.009

In both cases the difference between the adjustment value and the literature one in proved negligible and therefore is possible to consider for this analysis the tabular values.

To have a complete range of possibilities the ET_c was calculated in the following chapter using both the K_{cmid} of *Artemisia absinthium* (0.8) as well as the one of Sage (1) to consider the two extreme values of the lookalike herbaceous plant.

6. Precipitation Data Processing and Water Balance Assessment

Monthly precipitation statistics were obtained from ERA5-Land reanalysis data provided by the European Centre for Medium-Range Weather Forecasts (ECMWF) over the interest area of the region. ERA5-Land data provide land variables hourly on a regular grid with spatial resolution of 0.1° (around 9 km near the equator), from 1950 up to the present.

The last part of this project involved the total precipitation variable Tp, in water equivalent meters per time step, for July of every year from 1995 to 2024, obtained through a Python script.

All NetCDF files were manipulated using the xarray and rioxarray libraries in Python. Starting with a single file for every July of a year, Tp values were summed hourly for each month for each year to obtain the monthly precipitation sum. The fields obtained were scaled from meters to millimetres and converted into daily mean format by dividing by 31.

After verifying that all grids had identical spatial extent, projection (EPSG:4326 – WGS84), and coordinate reference system, the 30 consecutive annual July precipitation raster were tied together along a new time dimension (year). The multi-year stack was used to compute the multi-annual average precipitation (1995–2024) and finally, the outputs were exported as single-band GeoTIFFs with units of millimetres per day (mm/day).

The resultant maps are of a spatial resolution around 9 km and provide spatially continuous, physically consistent July precipitation estimates in the Aosta Valley.

This raster has been projected to EPSG:23032 (UTM 32N) to be in the same spatial reference of the ET_{\circ} map. Also resampling to common spatial resolution (2 m) for overlay analyses, as and when necessary, was performed.

The spatial distribution of July precipitation shows a clear altitudinal and orographic gradient in the Aosta Valley. The daily average precipitation ranges between approximately 2.1 mm/day in the lower parts of the valley and 6.3 mm/day in the northwestern mountainous areas, corresponding to approximately 65 to 195 mm/month, respectively. The 3.7 mm/day mean value at regional scale (around 115 mm/month) is consistent with the mean July climatology reported by ARPA Valle d'Aosta and WorldClim v2.1 datasets. The highest precipitation values are located above the Mont Blanc and Gran Paradiso, whereas the opposite is the driest along the central valley axis.

6.1. Water Deficit Calculation

To estimate the potential water deficit, the raster of mean precipitation (P) was subtracted from the raster of mean crop evapotranspiration (ET_c), both expressed in mm/day, following the Formula (25):

$$D = (ET_o \times k_{cmid}) - P \tag{25}$$

where *D* represents the daily water deficit.

Positive values (D > 0) indicate a water deficit, meaning evapotranspiration exceeds precipitation and irrigation may be required.

Values near zero represent approximate water balance.

Negative values (D < 0) indicate water surplus, when precipitation exceeds evapotranspiration.

Considering $K_c = 1$ (Sage)

The water condition of the fields is reported in the following table (Table 8):

Table 8. Water deficit conditions of all the existing fields using a K_{cmid} of 1.

Water deficit conditions	A.U. fields	values
High deficit	39 fields	From 1.16 to 2.05 mm/day
Moderate deficit	17 fields	From 0.30 to 0.95 mm/day
Surplus	15 fields	From 0 to -0.78 mm/day

Using the crop coefficient mentioned above, the water deficit condition in the area of interest assumes the following values (Figure 28) (Figure 29):

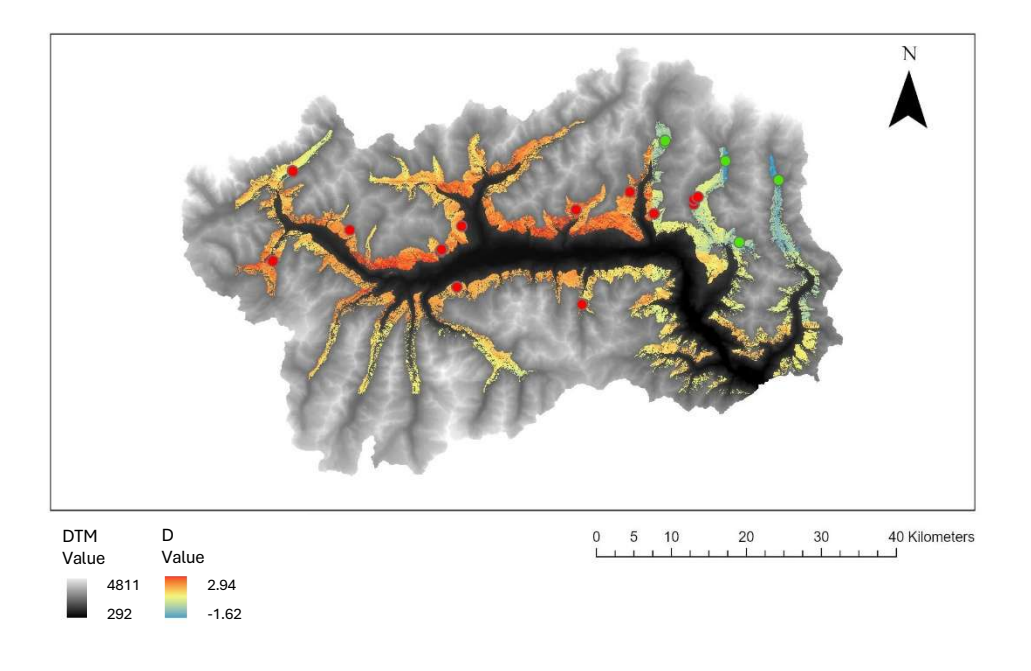


Figure 28. Visual representation of the water deficit in the study area [mm/day].

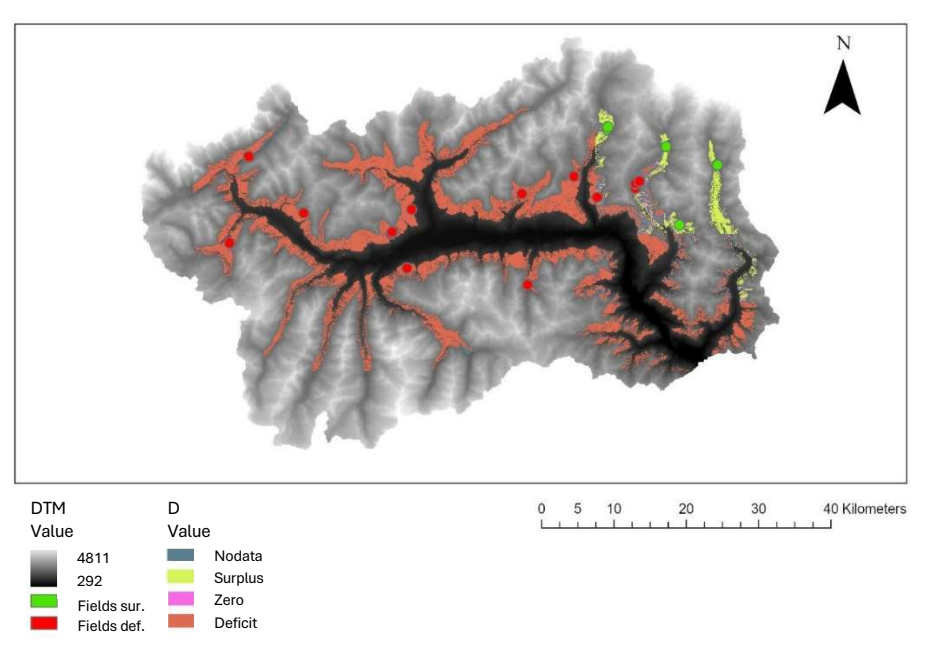


Figure 29. Visual representation of positive, negative and null D values in the area of agricultural interest.

Considering K_c=0.8 (Artemisia absinthium)

The water condition of the fields is reported in the following table (Table 9):

Table 9. Water deficit conditions of all the existing fields using a K_{cmid} of 0.8.

Water deficit conditions	A.U. fields	values
High deficit	12 fields	From 1 to 1.12 mm/day
Moderate deficit	30 fields	From 0 to 0.94 mm/day
Surplus	29 fields	From 0 to -1.6 mm/day

Using the crop coefficient mentioned above, the water deficit condition in the area of interest assumes the following values (Figure 30) (Figure 31):

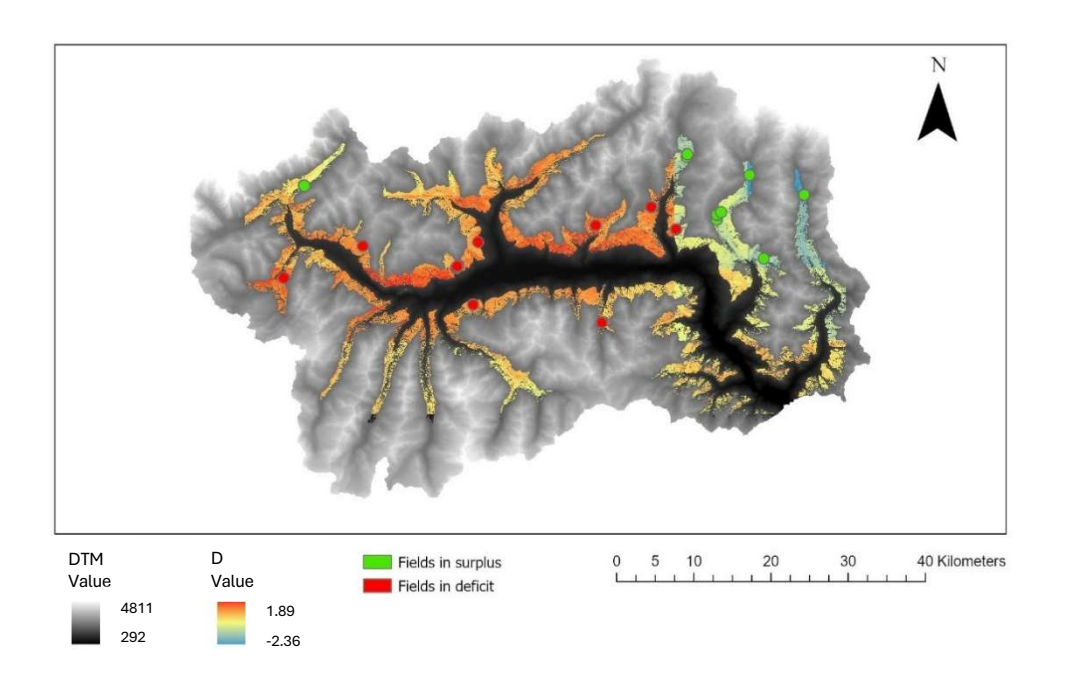


Figure 30. Visual representation of water deficit in the study area [mm/day].

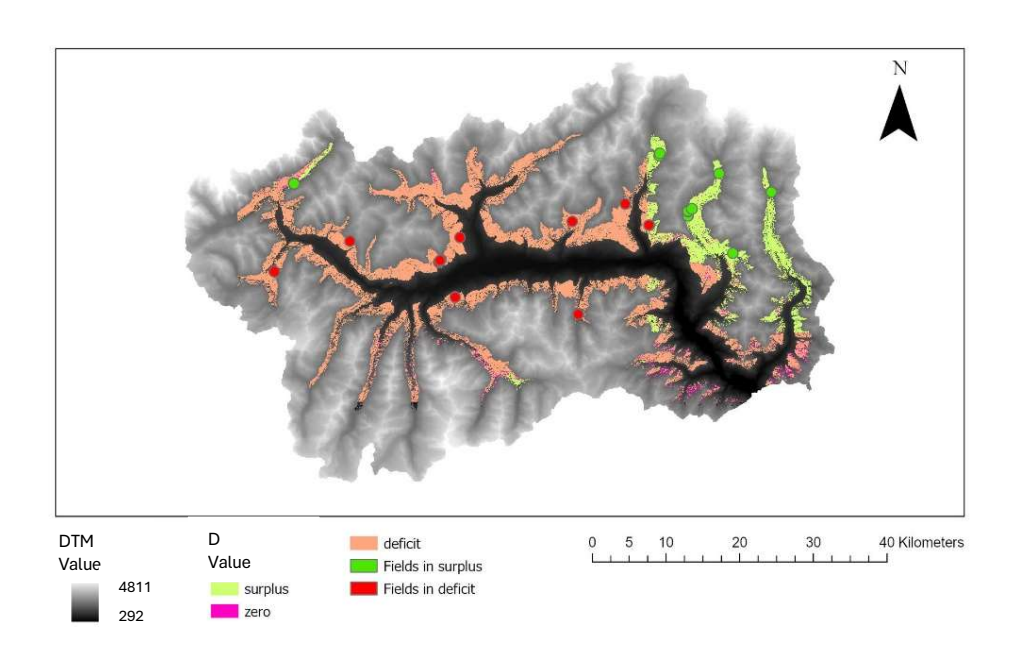


Figure 31. Visual representation of positive, negative and null D values in the area of agricultural interest.

6. Conclusion

This project combined the topography of the Aosta Valley region at 2 meters spatial resolution with realistic couple of atmospheric coefficients in each point of a 2km grid, to create very high-resolution solar radiation and reference evapotranspiration maps for studying the current cultivation of *Artemisia umbelliformis*. Thanks to a combined analysis of PVGIS radiation data and ArcGIS Pro solar tools, these maps consider slope, aspect, and topographic shading as well as the atmospheric parameters, representing in a very realistic way the climatic variable and the eco-climatic one, trying not to leave out significant parts of the alpine landscape that strongly affect results.

Results

The modelling of the atmospheric parameters (*ti* and *di*) at the local level relying on PVGIS data created a fundamental basis to produce very accurate radiation fields adequately representing the intricate relief of the valley.

In January, A.U. fields receive more solar energy compared to the rest of the area of agricultural interest and have a reference evapotranspiration demand that is almost double the average for the territory. This indicates favorable exposure and microclimatic conditions.

In summer, both R_s and ET_o values remain higher than the total area, but the difference is less marked than in winter: in summer, the entire territory reaches high values, and the differences are reduced. A.U. existing cultivation fields are ideal micro-areas.

By approximating the crop coefficient to the ones of similar aromatic herbs, *Artemisia absinthium* and *Salvia officinalis*, the calculation of the crop evapotranspiration was achieved. This allowed the analysis field-by-field of the water deficit, considering precipitation data (ERA5-Land), and the necessity of irrigation which is, in fact, necessary for most fields in July, in both cases of k_c.

Overall, the results confirm the conclusion of Aguilar, Herrero and Polo, 2010: in the high mountain environment, topography is the main factor that determines the radiation distribution and therefore the Eto.

Strengths and limitations

The devised methodology represents a new workflow applicable to many other alpine or aromatic crops, identifying with high accuracy the water balance and the suitability of the cultivation area. The integration of spatially and temporally calibrated parameters provides a realistic calculation of energy and water fluxes compared to the traditional approaches based on interpolation.

However, some approximations, such as the R_s/R_{so} relationship and the use of standardized atmospheric pressure equations proposed by FAO, should be refined. Additionally, the analysis was conducted only for January and July: it would be interesting extend the analysis to all the months to produce a continuous annual ET_o or at least, for this specific plant, to June, August and September to analyzed the water deficit also with K_{cin} and K_{cend} .

Future perspective

To strengthen and expand the model several directions can be taken:

- Enter production data of the A.U. fields to directly correlate biophysical variables with agricultural productivity.
- Improve the temperature resolution through interpolation, as there is a high correlation between this variable and altitude, which is available at very high resolution.
- Improve K_c estimation by measuring it in the fields or figuring it out through experiments.

• Improve the resolution of precipitation data to have even more detailed D.

General conclusions

In conclusion, this research demonstrates that by correctly combining topographic solar modeling, atmospheric calibration, and evapotranspiration calculations following the FAO manual, a robust resource is obtained to aid sustainable agriculture in mountainous regions. In addition to its scientific value, this method provides already practical advice for crop location planning and irrigation control.

With further future improvements such as those outlined above, this framework could evolve into a decision-support system for precision agriculture, by incorporating remote-sensing data and field-sensor information to increase the resilience and productivity of mountainous ecosystems.

Bibliography

Allen R.G., Pereira L., Smith M., Raes D., Wright J., *FAO-56 Dual Crop Coefficient Method for Estimating Evaporation from Soil and Application Extensions*, Journal of Irrigation and Drainage Engineering, 131(1), 2005.

Binet M.-N., van Tuinen D., Deprêtre N., Koszela N., Chambon C., Gianinazzi S., *Arbuscular mycorrhizal fungi associated with Artemisia umbelliformis Lam., an endangered aromatic species in the Southern French Alps, influence plant P and essential oil contents*, Mycorrhiza, 21, pp. 523–535, 2011.

Bosquilia R.W.D., Neale C.M.U., Longhi S.J., Ferraz S., Muller-Karger F.E., McCurthy M., *Evaluation of evapotranspiration variations as a function of relief and terrain exposure through multivariate statistical analysis*, Ecohydrology & Hydrobiology, 19, pp. 307-315, 2019.

Chow A., Fung A.S., Li S., GIS Modeling of Solar Neighborhood Potential at a Fine Spatiotemporal Resolution, Buildings, 4(2), pp. 195–206, 2014.

Comino C., Pignata G., Portis E., Dolzhenko Y., Casale M., Nicola S., *Selection in Artemisia umbelliformis Lam. Piedmont ecotypes to improve cultivation in alpine environment*, Genetic Resources and Crop Evolution, 62(4), pp. 567–577, 2015.

Dubayah R., Rich P.M., *Topographic Solar Radiation Models for GIS*, International Journal of Geographic Information Systems, 9, pp. 405–413, 1995.

Erschbamer B., Retter V., *How long can glacier foreland species live?*, Flora, 199(6), pp. 500–504, 2004.

Fontaine N., Gauthier P., Caillon S., Thompson J., Boulangeat I., *Sustainability of Artemisia umbelliformis gathering in the wild: an integration of ecological conditions and harvesting exposure*, Global Ecology and Conservation, 51, e02886, 2024.

Hofierka J., Šúri M., *The Solar Radiation Model for Open Source GIS: Implementation and Applications*, Proceedings of the Open Source GIS–GRASS Users Conference, Trento, 2002

Körner C., *Alpine Plant Life: Functional Plant Ecology of High Mountain Ecosystems*, Springer, 2003.

Körner C., *Coldest places on earth with angiosperm plant life*, Alpine Botany, 121, pp. 11–22, 2011.

Li J., Heap A.D., *Spatial interpolation methods applied in the environmental sciences: A review*, Environmental Modelling & Software, 53, pp. 173–189, 2014.

Pereira L.S., Mota M., Raziei T., Paredes P., Water requirements and crop coefficients of edible, spicy and medicinal herbs and vegetables: a review aimed at supporting plant and water management, Irrigation Science, 42, pp. 1199–1228, 2024.

Raaflaub L.D., Collins M.J., *The Effect of Error in Gridded Digital Elevation Models on the Estimation of Topographic Parameters*, Environmental Modelling & Software, 21(5), pp. 710–732, 2006.

Rey C., Mercanti B., Bondaz F., Bonfanti R., Lini U., Plott S., Piantini U., Gaillard F., Theodoloz G., Grogg A.-F., *Projet interrégional sur la culture du génépi blanc*, Revue suisse de viticulture, arboriculture, horticulture, 34(5), pp. 325–337, 2002.

Smith, M., Segeren A., Santos Pereira L., Perrier A., Allen R., Report on the expert consultation on procedures for revision of FAO guidelines for prediction of crop water requirements, FAO, Rome, 1990.

Šúri M., Hofierka J., *A New GIS-Based Solar Radiation Model and Its Application to Photovoltaic Assessments*, Transactions in GIS, 8, pp. 175–190, 2004.

Zotarelli L., Dukes M.D., Romero C.C., Migliaccio K.W., Morgan K.T., *Step by Step Calculation of the Penman–Monteith Evapotranspiration (FAO-56 Method)*, University of Florida, AE459, 2010.

Web references

Climate-Data.org, *Climate averages for Aosta, Italy (temperature, precipitation, humidity, rainy days, etc.)*, retrieved October 2025, from https://en.climate-data.org/europe/italy/aosta-valley/aosta-3041/

Copernicus Climate Change Service (C3S), *ERA5-Land hourly data from 1950 to present*, retrieved October 2025, from https://cds.climate.copernicus.eu/datasets/reanalysis-era5-land?tab=overview

ESRI, *Mapping & Analytics Software and Services*, retrieved February 2021, from https://www.esri.com/en-us/arcgis/about-arcgis/overview

European Commission – Joint Research Centre, *PVGIS: Photovoltaic Geographical Information System*, retrieved October 2025, from https://re.jrc.ec.europa.eu/pvg tools/en/#MR